

RICE UNIVERSITY

**Tailoring Vertically-Aligned Carbon Nanotube Growth for
Poly(dimethylsiloxane)-Infiltrated Nanocomposites**

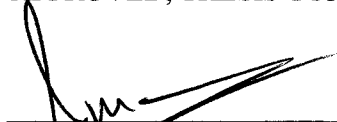
by

Brent J. Carey


A THESIS SUBMITTED
IN PARTIAL FULFILLMENT OF THE
REQUIREMENTS FOR THE DEGREE

Master of Science


APPROVED, THESIS COMMITTEE



Pulickel M. Ajayan, Chair
Benjamin M. and Mary Greenwood
Anderson Professor of Engineering



Enrique V. Barrera
Professor of Mechanical Engineering &
Materials Science, Chair



Carl Rau
Professor of Physics & Astronomy

HOUSTON, TEXAS
April 2010

UMI Number: 1486019

All rights reserved

INFORMATION TO ALL USERS

The quality of this reproduction is dependent upon the quality of the copy submitted.

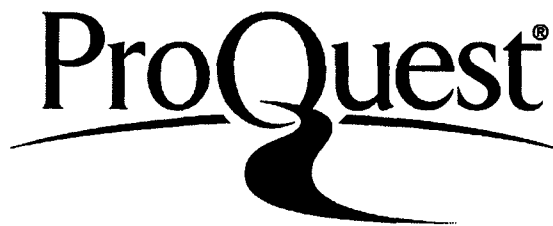
In the unlikely event that the author did not send a complete manuscript and there are missing pages, these will be noted. Also, if material had to be removed, a note will indicate the deletion.



UMI 1486019

Copyright 2010 by ProQuest LLC.

All rights reserved. This edition of the work is protected against unauthorized copying under Title 17, United States Code.



ProQuest LLC
789 East Eisenhower Parkway
P.O. Box 1346
Ann Arbor, MI 48106-1346

Abstract

Tailoring Vertically-Aligned Carbon Nanotube Growth for Poly(dimethylsiloxane)-Infiltrated Nanocomposites

by

Brent Carey

This thesis discusses the viability of the polymer infiltration nanocomposite preparation technique for aligned carbon nanotubes (A-CNTs) as produced by two methods: pre-deposited catalyst chemical vapor deposition (CVD), and vapor-phase CVD. Both types of growth furnaces were constructed, and the resultant A-CNT “forests” were impregnated with poly(dimethylsiloxane), a highly-compliant silicone elastomer. The survivability of the CNT alignment subsequent to the polymer infiltration was studied for the respective nanocomposites, and it was observed that the thin-walled CNTs produced by the pre-deposited catalyst CVD method were not robust enough to maintain alignment during the infiltration, in contrast to the thicker-walled vapor-phase-grown CNTs. The dynamic mechanical properties of the successfully-impregnated composites were then studied, and their strain- and frequency-dependent behavior was probed both transverse and longitudinal to the alignment direction of the CNTs, revealing distinct responses due to their anisotropy.

Acknowledgments

I'd like to take this opportunity to personally thank those who have assisted me so far in my graduate studies. Firstly, I'd like to extend gratitude to my advisor, Professor Pulickel M. Ajayan, as he has been the driving force behind my research. In addition to his expertise in the field of carbon nanotubes, I appreciate his "open door" policy and constant encouragement. I'd also like to thank the other members of my committee, Professors Enrique Barrera and Carl Rau, for taking the time to understand my work and providing the feedback which is critical to my growth as a scientist.

Much thanks go to Dr. Lijie Ci, who trained me not only on the art of nanotube synthesis, but as well on the method of infiltrating the CNT forests with a polymer. Also, Professor Prabir Patra of the University of Bridgeport is to thank for his constant attention to my work as well as his foresight to procure the DMA which has proven to be a cornerstone of my research. I look forward to working with them both for the extent of my time at Rice and perhaps beyond.

I'd like to acknowledge NASA and particularly the Graduate Student Researchers Program (GSRP) for their financial support of my work.

Lastly, but certainly not least, I'd like to thank my wife, Sarah, for her unwavering support and for being willing to relocate to Texas so that I can pursue my degree. For this and many other reasons, I wouldn't be where I am today without her.

Contents

Acknowledgments	iii
Contents	iv
List of Figures	vi
List of Tables	viii
Introduction	1
1.1. Introduction to Carbon Nanotubes.....	1
1.2. Techniques in Carbon Nanotube Synthesis	3
1.2.1. Early Carbon Nanotube Synthesis Methods	3
1.2.2. Chemical Vapor Deposition to Produce Aligned CNTs	5
1.3. Carbon Nanotubes for Composite Applications	7
1.3.1. Challenges in Preparing Randomly-Aligned Nanocomposites.....	7
1.3.2. Self-Assembly of CNTs to Achieve Composite Homogeneity	9
1.4. Research Motivations.....	10
Synthesizing Aligned Carbon Nanotube Arrays for Composite Applications	12
2.1. Pre-Deposited Catalyst CVD	13
2.1.1. Introduction to Pre-Deposited CVD Growth.....	13
2.1.2. Construction of a Water-Assisted A-CNT Growth Furnace.....	14
2.1.3. A-CNTs Grown Via Pre-Deposited Catalyst CVD	19
2.2. Vapor-Phase CVD	22
2.2.1. Introduction to Vapor-Phase CVD Growth	22
2.2.2. Construction of a Vapor-Phase A-CNT Growth Furnace.....	23
2.2.3. A-CNTs Grown via Vapor-Phase CVD	29
2.3. Comparison of A-CNTs for Infiltrated Composite Applications	33
Vertically-Aligned Carbon Nanotube/ Poly(dimethylsiloxane) Composites	35
3.1. Introduction to Poly(dimethylsiloxane)	36
3.2. Composite Preparation	37
3.2.1. Results from Pre-Deposited Catalyst A-CNT Infiltration.....	38
3.2.2. Results from Vapor-Phase A-CNT Infiltration	39

3.3. Dynamic Mechanical Properties of A-CNT/PDMS Composites.....	40
3.3.1. Strain Sweep	42
3.3.2. Frequency Sweep.....	46
3.3.3. Temperature Ramp.....	48
Conclusion and Future Work.....	50
References	52

List of Figures

Figure 2.1 – Schematic of pre-deposited CVD growth substrate (not to scale).	16
Figure 2.2 – Bank of mass flow controllers and water bubbler.....	17
Figure 2.3 – Schematic (a) and photograph (b) of the pre-deposited catalyst CVD system.....	18
Figure 2.4 – Growth height as a function of water vapor content.....	20
Figure 2.5 – Water-Assisted Pre-Deposited Catalyst CNTs.....	21
Figure 2.6 – Continuous pump, xylene/ferrocene mixture, and mass flow controllers for vapor-phase CVD.....	24
Figure 2.7 – Photographs of the coaxial gas/liquid delivery (a), evaporator cap (b) and its seat (c), and schematic of gas flow around evaporator (d).	27
Figure 2.8 – Schematic (a) and image (b) of the vapor-phase CVD system.....	28
Figure 2.9 – Schematic of vapor-phase CNT thickness as a function of growth height [44].	30
Figure 2.10 – Photograph of A-CNTs grown via vapor-phase CVD.....	30
Figure 2.11 – TEM images of the “top” (a,b), “middle” (c,d), and “bottom” (e,f) of xylene/ferrocene A-CNTs.	31
Figure 2.12 – SEM images of the “top” (a,b), “middle” (c,d), and “bottom” (e,f) of xylene/ferrocene A-CNTs.....	32
Figure 3.1 – Molecular structure of PDMS [47].....	36
Figure 3.2 – SEM image of poor alignment in pre-deposited catalyst composite.	39
Figure 3.3 – SEM image of the good polymer/CNT physical interaction and CNT alignment for vapor-phase A-CNT/PDMS composites.	40
Figure 3.4 – Schematic of axial dynamic compression on the A-CNT composites.	42

Figure 3.5 – Schematic of the axial (a), radial (b), and neat polymer (c) samples, and a SEM image (d) of the samples used for DMA testing.	43
Figure 3.6 – Storage and loss moduli (a) of a strain sweep DMA test. Schematics showing the radial (c) and axial (d) displacement of the CNTs under strain.	45
Figure 3.7 – Tangent delta for a frequency sweep DMA test.....	47
Figure 3.8 – Temperature ramp showing the glass transition (a) and thermal degradation (b) of the composite vs. the neat polymer.	49

List of Tables

Table 2.1 - Parameters for optimal water-assisted CVD growth.....	17
Table 2.2 - Parameters for vapor-phase CVD growth.....	29

Chapter 1

Introduction

1.1. Introduction to Carbon Nanotubes

Due to their impressive array of properties, carbon nanotubes (CNTs) have received a substantial amount of attention since the landmark paper in 1991 which brought them to prominence [1]. In the nearly two decades since their naissance, CNTs have been explored in a wide range of applications ranging from field emission [2], capacitors [3], hydrogen storage [4], chemical sensing [5], thermal management [6], and even as axles in nanoscale vehicles [7].

The application of CNTs for these purposes is owed to the truly impressive properties of these molecules. They are reported to have a thermal conductivity up to $6,600 \frac{W}{m-K}$ at room temperature [8], have been shown to be capable of exhibiting ballistic electrical conduction [9], and can have axial mechanical strength on the order of 1 TPa [10], properties which are head-and-shoulders and, in some cases,

even orders-of-magnitude above other materials. As such, CNTs have been lauded as some of the most perfect molecules that could exist.

CNTs come in a range of sizes and morphologies, each with its own specific electronic, thermal, and mechanical properties; this, in itself, is a testament to the collective value of these molecules in future applications. These allotropes range from single-walled (SWNTs) to multi-walled CNTs (MWNTs), with a few special subsets such as double-walled (DWNTs) and few-walled CNTs (FWNTs). Adding to this complexity, each of these come in a range of helicities (termed a CNT's "chirality"), though this characteristic is typically only used when referring to SWNTs; the chirality of a SWNT can determine metallic or semimetallic behavior, and isolating each of these types of SWNTs is the subject of research focus to this day [11].

Additionally, the idealized properties reported for CNTs generally assume a perfect crystalline structure. Unfortunately, despite great efforts, highly-crystalline CNTs are not experimentally viable in large quantities even by present day growth procedures. Due to inherent difficulties in synthesis, even the CNTs generated by today's highly-optimized methods are typically produced in a small yield of highly-crystalline CNTs or a large yield of highly-defective CNTs, with some processes falling in the middle of those two extremes. Research still continues to perfect these growth processes.

Given all of this, the CNTs produced in large quantities still have significant utility. Despite their non-perfect structure, they are typically much cheaper to

produce and still exhibit impressive properties as compared to many other materials. The work presented herein is based upon such CNTs, as produced through chemical vapor deposition (CVD).

1.2. Techniques in Carbon Nanotube Synthesis

Over the course of the 1990's, several novel synthesis methods were devised, and most of those techniques have been refined over the past decade and are still in use today to produce CNTs for specific research, industrial, and commercial needs. As described previously, CNTs come in many varieties. Each of these synthesis methods produces its own "fingerprint" of CNTs, which is typically a distribution of certain CNT types and sizes. For specific applications, the synthesis technique is typically selected by the quantity, quality, and size/chirality of the desired material. Below, I summarize the major milestones in CNT synthesis, and delineate each technique's successes and shortcomings.

1.2.1. Early Carbon Nanotube Synthesis Methods

Arc-Discharge was the first technique used to deliberately produce CNTs, as reported by Iijima in 1991 [1]. The yield of CNTs by this process was quite low, though they are typically of very high crystallinity. A few years later, Ebbeson & Ajayan expanded upon the arc-discharge method to produce gram quantities of these CNTs [12], which include both SWNTs and MWNTs with lengths of up to 50 μm . By their method, $\sim 18\text{ V}$ (AC or DC) is applied across two graphitic rods in a 500 Torr helium atmosphere. When the two electrodes are brought close enough to

arc, 100 A of current passes between them, creating a plasma which provides a nucleating environment for CNTs. To this day, arc-discharge is still a preferred method for ultra-high-quality CNTs if there is little concern about length, though other methods have since surpassed it in producing much larger quantities.

In 1993, José-Yacamán et al. reported the first use of CVD for the expressed purpose of synthesizing CNTs [13]. The CVD process generally involves the use of a hydrocarbon gas which decomposes in a high temperature environment, producing the feedstock carbon for CNT synthesis. When placed in a sufficient but not excessive temperature environment (generally $\sim 700 - 900$ °C), catalyst particles of certain transition metals will begin to consume any available carbon and initiate the growth of CNTs. In this last-referenced work [13], acetylene was passed over a substrate covered with iron particles in a 700 °C atmosphere, resulting in the growth of CNTs up to 50 μm in-length. Shortly after, Endo et al. were able to initiate the use of a vapor-phase catalyst to synthesize pyrolyzed CNT structures by adapting a procedure similar to what is used to create vapor-grown carbon nanofibers (VGCNFs) [14]. By passing benzene over a carbon block in a hydrogen-rich environment at 1000 °C, highly-graphitic CNTs and CNT-like structures were generated. CVD is also responsible for the high-pressure CO (HiPCO) growth method developed by Nikolaev et al. in 1999, which has allowed for the large-scale production of SWNTs [15]. Due to its relative ease, there have been many variations on the CVD synthesis of CNTs which have brought it to prominence as a simple, yet effective method to produce large quantities of CNTs.

In 1995, Smalley and co-workers reported the laser ablation technique [16], which benefits from a much larger and predominantly SWNT yield. After vaporizing a graphitic carbon / transition metal target with a laser in the presence of an inert gas, the carbon will condense on cool surfaces in the reaction chamber, where CNTs will begin to form. Despite its efficiency in producing large quantities of quality CNTs, this technique is largely overlooked due to its prohibitive cost.

The majority of the CNT synthesis work over the rest of the 1990's and 2000's was focused on understanding and refining the above methods to both improve the quality and/or reduce the size distribution of these methods while scaling up the production. These efforts have helped to expand CNT production into the private sector, where the quality has improved significantly and the cost-per-gram of CNTs has steadily dropped.

1.2.2. Chemical Vapor Deposition to Produce Aligned CNTs

One of the particularly interesting aspects of CVD is the ability to use this method to synthesize self-aligned "forests" of carbon nanotubes (A-CNTs), as first reported in 1996 by Li et al. [17]. The CNTs produced were exclusively MWNTs and measured approximately 40 μm in-length. Another evolution of the CVD technique to grow A-CNTs, perhaps fueled by the success of the arc-discharge method, was the introduction of a plasma source, as first reported in 1997 [18]. Their procedure allowed for a lower growth temperature and the use of a much less specialized substrate. In the mid 2000's, Hata and co-workers developed a technique they termed "supergrowth" which involved the introduction of water vapor during the

CVD growth procedure [19]. Spawned by a report that an amorphous carbon coating on the catalyst particles was “poisoning” them and terminating the growth [20], their supergrowth procedure helped to produce a reducing environment inside the reaction chamber which cut down on amorphous carbon and lead to the growth of A-SWNT forests up to 2.5 mm long. Later, Amama et al. suggested that the success of water in the supergrowth procedure was owed to the decoration of the inter-catalyst substrate space with hydroxide species, thereby stifling the Ostwald ripening of the catalyst particles in the high temperature growth environment [21]. Further refining of this water-assisted technique in the recent past has lead to the growth of forests up to 5 mm tall, and the discovery that the continuous flow of water vapor during the cool-down of the furnace after growth will serve as a weak oxidizer which will cause the CNTs to detach from the substrate, leaving a free-standing film of CNTs [22].

CVD is a method which has been considerably improved in the decade-and-a-half since its inception as a CNT synthesis method, and is the favored method for producing very large quantities due not only to the scalability of the procedure, but also its low cost. Unfortunately, while advances have been made, it is still not nearly as effective in producing top-quality CNTs as the other common methods.

In Chapter 2, I will describe the CVD procedures for growing A-CNT arrays with more depth, and will specifically describe the methods used to produce the aligned CNTs for this work.

1.3. Carbon Nanotubes for Composite Applications

1.3.1. Challenges in Preparing Randomly-Aligned Nanocomposites

No matter the matrix material one is attempting to reinforce with CNTs or any nanoscale material, the greatest challenge in nanocomposite preparation is arguably in dispersion. While surface-area-to-mass ratio is the origin of their advantage over traditional materials, it is the predominant factor which leads to the agglomeration of nanomaterials. CNTs are no exception to this, as they have been observed to readily form rope-like structures both after growth and in solution; these CNT ropes are very difficult to break apart due to the Van der Waals attraction between such atomically pristine surfaces, and the use of strong acids such as fuming sulfuric acid (oleum) is one of the only methods by which to intercalate these dense bundles [23].

Agglomeration is a real issue in the manufacturing of nanocomposites, and for more than one reason. Firstly, the special properties of these nanomaterials are largely dependent on their size and/or structure. When they agglomerate and aren't homogeneously dispersed in a particular medium, much of their advantage is lost. Along those lines, while they are remarkably difficult to separate, the interactions between these nanoparticles are inherently weak since the attraction is predominantly orthogonal to the surface. Put simply, agglomerates are highly susceptible to shear forces and can easily slide past each other. Inside of a matrix, such sliding significantly threatens the bulk structural integrity under loading. This issue is amplified for CNTs due to their extremely high aspect ratio (eg. 10,000: 1 for

a .5 mm long, 50 nm in-diameter CNT). CNTs bundled into ropes are extremely difficult to separate, and can slide past each other with very little effort. Such mobility has cast some doubt on the use of randomly-dispersed CNTs as effective reinforcement in nanocomposites, and is one of the reasons given as to why nanocomposites have not yet achieved the theoretical predictions for their potential [24].

Despite these difficulties, many have attempted to use CNTs to reinforce both stiff and compliant matrices. While there exist some reports on the topic of their use in reinforcing metals [25] and metal-oxides [26], the vast majority of work using CNTs as mechanical reinforcement in composite materials has been by the way of polymer matrices. The first report of CNTs in a polymer matrix was in 1994, where Ajayan et al. showed that the cutting of an epoxy/CNT composite could result in the alignment of the CNTs embedded in the matrix [27]. Four years later, Wagner and co-workers reported the first mechanical properties of a CNT/polymer composite by spreading a urethane/diacrylate oligomer on a dried film of MWNTs prior to UV-curing [28]. It wasn't until the following year when Jia et al. attempted to create a bulk composite by dispersing as-grown CNTs in a poly(methyl methacrylate) matrix through mixing [29]. Despite sufficient stirring, they reported large clusters of CNTs due in part to the reasons described previously regarding agglomeration.

Compounding the problems due to agglomeration, even dispersion in a matrix is also somewhat hindered by the viscosity of the medium. Methods such as ball mixing and extrusion have been reported as means by which to more-evenly

disperse CNTs into metal [30] and polymer [31] matrices, respectively. While many have reported success with such procedures, there still exist concerns about the survivability of the CNTs through such forceful methods [32].

Due to their gas permeability, another option for increased homogeneity specifically in polymer matrices is through the use of surfactants; by lowering the viscosity of the matrix through the “lubrication” of the polymer chains, the CNTs are able to more-easily intercalate and spread homogeneously throughout the matrix. Gong et al. were the first to report solvent addition to this end for CNT composites [33], where they reported that the composite prepared with a solvent had a much more significant shift in the glass transition (T_g) and a 30% increase in the elastic modulus as compared to the traditionally-prepared control. They did note, however, that agglomeration of the CNTs was still an issue. Over the following decade, the use of solvents has become a favored technique for the manufacturing of randomly-dispersed nanocomposites due to the ease of solvent removal after dispersion has taken place.

1.3.2. Self-Assembly of CNTs to Achieve Composite Homogeneity

As it can be very difficult to break apart aggregates and then evenly disperse nanoscale constituents in a matrix, a more favorable technique would be to organize the CNTs prior to introducing the polymer. This was, in fact, the technique used in the early days of CNT composite study, where randomly-aligned films of CNTs were created through the dispersion in a solvent and subsequent filtering or evaporation [28]. While this does provide a backbone for a two-dimensional composite film, the

true challenge is in organizing CNTs three-dimensionally. Such a feat is no trivial task, as it is not physically feasible to organize such a large number of individual CNTs. As such, the only viable way to achieve such spatial organization is through self-assembly.

As mentioned in Section 1.2.2, CVD can be used to grow vertically-aligned arrays of CNTs whose spacing and orientation are predefined by the growth conditions. In contrast to the typical method of introducing CNTs to a polymer, the success of this method lies in introducing the polymer to these already-oriented CNT arrays. This technique of polymer infiltration was first explained in-depth in 2005 through the infiltration of methyl methacrylate prior to polymerization [34]. Assuming there is sufficient surface interaction (wetting) between the CNTs and the desired matrix (a surface wetting study between CNTs and many common matrix polymers is given in a report by Barber et al. [35]), this method of composite preparation is as trivial as infiltrating the aligned forest with the matrix polymer prior to crosslinking (for curable polymers), with or without the use of a solvent. A similar polymer infiltration method was the technique used for this thesis work, and specific details are given in Section 3.1.

1.4. Research Motivations

While there has been much research on the development of CNT-reinforced composites, there are still very significant issues with agglomeration and dispersion. This is particularly true for very-large-aspect-ratio CNTs, which become virtually

impossible to homogeneously disperse in any sort of composite matrix. A-CNTs provide an ideal solution to these problems, as the spacing of the CNTs is near ideal to allow for effective infiltration while allowing for significant improvement over the neat polymer. As such, it is necessary to ascertain the ideal CNTs for such an application and to explore the properties of such continuously-reinforced composites. The present thesis will attempt to solve the following problems:

1. For two types of A-CNT growth (pre-deposited catalyst CVD and vapor-phase CVD), how can the parameters be optimized to ensure consistent growth with the expressed purpose of using those A-CNTs for infiltrated composite applications?
2. How do both types of A-CNTs react to the infiltration of a polymer matrix? Can they maintain their alignment/anisotropy?
3. How do the A-CNT composites react to dynamic mechanical stimulus? What can this type of testing tell us about the subtle structural and morphological properties the CNTs are imparting on the matrix polymer?

Synthesizing Aligned Carbon Nanotube Arrays for Composite Applications

There are two primary techniques for the CVD production of A-CNTs, and each comes with its own strengths and weaknesses depending on the desired application of the end product. The main distinction between the two lies in how the catalyst is introduced to the system, and the manner in which it interacts with the carbon source.

For this thesis work, two separate growth furnaces were constructed and the resultant growth products from both were compared for viability as reinforcement in vertically-aligned CNT nanocomposites. In this chapter I will discuss the differences between these two techniques and highlight my observations of their drawbacks and successes for the production of A-CNTs for composite applications.

2.1. Pre-Deposited Catalyst CVD

2.1.1. Introduction to Pre-Deposited CVD Growth

The earliest method of A-CNT production involved the use of a substrate pre-deposited with the catalyst particles used for CNT synthesis [17]. The deposition of the catalyst can be accomplished by a few techniques, including sputter coating and electron-beam evaporation.

The technique of pre-depositing the catalyst prior to growth has a few gains over trying to deliver the catalyst in the vapor phase; when the catalyst is deposited on the surface prior to synthesis, the resultant CNTs generally have a much narrower distribution of sizes. The thickness of this catalyst layer (generally between .5 and 5 nm thick) will largely will define the diameter of the resultant CNTs, giving some control over the types of CNTs synthesized [22]. Also, as the amount of catalyst is tightly controlled, there are fewer growth parameters to optimize, typically providing more consistent, repeatable growth. Another success of this technique lies in the complex growth surfaces which can be engineered. Custom masks can be used to selectively determine where the catalyst will be deposited, and CNT growth normal to these surfaces can be used to grown 2D patterns such as towers [36].

Despite these strengths, the main shortcoming of this method lies in the preparation that needs to be done to the substrate in order to grow CNTs. The success of the growth is dependent on the application of the catalyst particles, which

makes it very difficult to grow CNTs on anything other than simple, relatively planar substrates such as silicon wafers.

2.1.2. Construction of a Water-Assisted A-CNT Growth Furnace

The first step in pre-deposited catalyst CNT synthesis is having a sufficiently hot reaction zone in order to initiate CNT nucleation. This is typically done through the use of a tube furnace, where these temperatures can be achieved while assuring even, laminar flow of the reaction gases over the substrate to limit growth inconsistencies due to turbulence. Due to the sensitivity of the growth process, having a consistent temperature profile across the desired growth zone is of paramount concern. For this reason, long tube furnaces are generally used for applications where the growth is to occur over a large area, as the longer the furnace, the more even the temperature in the center region, leading to more consistent overall growth. For this work, a Thermolyne 79400 tube furnace with a 26" heating zone which can accommodate a 2" in-diameter quartz reaction tube was used.

The beauty of the pre-deposited catalyst growth method lies in its relative simplicity. Since the catalyst is already deposited on the substrate prior to synthesis, all one needs to be concerned with is the environment of the reaction zone and the flow of each gas used. However, since the kinetics of CNT synthesis are so complicated and difficult to predict, tight, repeatable control over every aspect of the reaction is essential. As the substrate for growth, silicon wafers pre-deposited with the catalyst were used as described in Figure 2.1. 1.5 nm of iron was

previously reported as producing the smallest distribution of CNTs via this method with a predominantly DWNT yield [37], so it was chosen as the preferred catalyst thickness for the growth of these CNTs with a 10 nm barrier layer of aluminum between it and the silicon wafer to prevent catalyst migration into the substrate. These metals were all deposited on the silicon wafer via e-beam evaporation.

To efficiently control the flow of each gas through the tube furnace, mass flow controllers (MFCs) were used; MFCs allow for tight, repeatable control over the flow of gases as compared to analog “turn-dial” flow controllers. Three MKS M100 MFCs controlled by a MKS Type 247 Four-Channel Readout were banked together (Figure 2.2) and used for this growth furnace to control the flow rates; these gases include the hydrocarbon reaction gas (ethylene), the gas flowed through the bubbler to pick up water vapor (15 vol% hydrogen, balance argon), and the gas which carries the reaction gases through the furnace (15 vol% hydrogen, balance argon).

With the furnace setup fully assembled as seen in Figure 2.3, the next step was to develop a consistent growth procedure. Based off of previous work [37] and with considerations taken during preliminary growth attempts, the following growth procedure was adopted:

1. Begin flowing the “carrier gas” (Q_c) and heat furnace up to the “introduction temperature” (T_i).
2. When stable, place substrate into the center of the growth zone and begin heating to the desired set point for the “synthesis temperature” (T_s).

3. At the exact time the set point is reached, begin flow of “bubbler gas” (Q_b) through water bubbler.
4. After bubbling for the desired “bubbling time” (t_b), initiate the flow of the “hydrocarbon gas” (Q_h).
5. After the desired “synthesis time” (t_s) has elapsed, bypass the bubbler through the three-way valve and turn off all but the Q_b during cool down.

Step 1 of the growth procedure was necessary in order to be sure that the substrates were all entered into the furnace at the same temperature and that they would be exposed to the growth atmosphere during heat-up for the same amount of time from run-to-run. If a free-standing mat of CNTs is desired, the Q_b can be left flowing through the bubbler after the carbon source is turned off and before cool down, where the added vapor can act as a weak oxidant and cause the CNTs to release from the substrate [22].

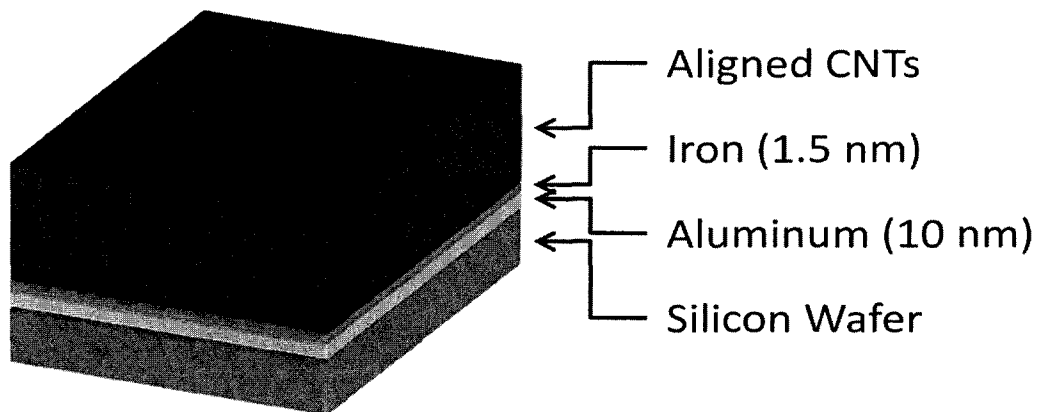


Figure 2.1 – Schematic of pre-deposited CVD growth substrate (not to scale).

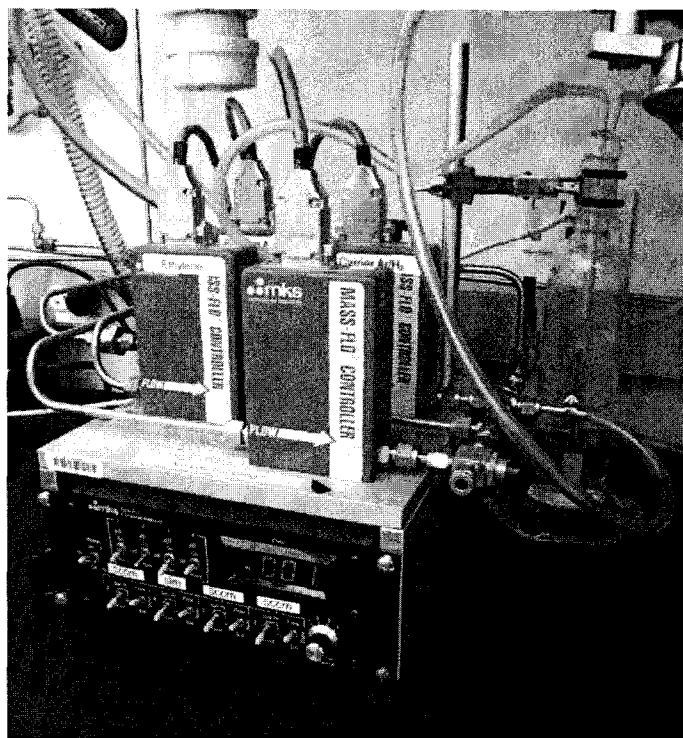
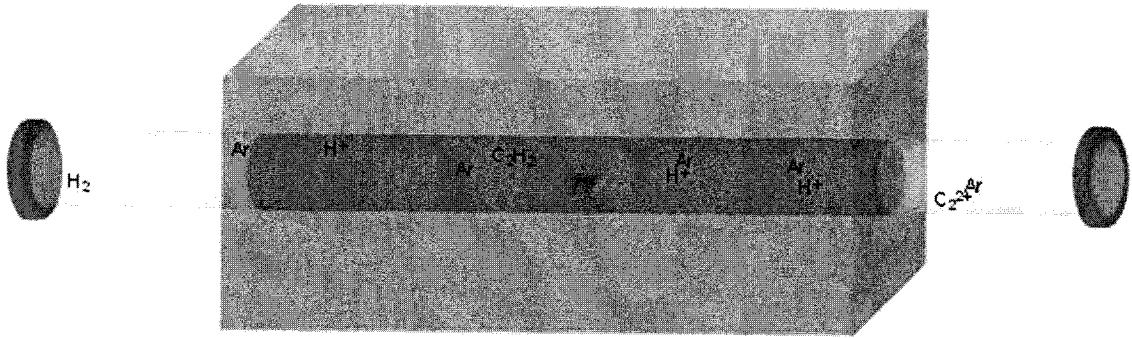


Figure 2.2 - Bank of mass flow controllers and water bubbler.

T_i (°C)	T_s (°C)	t_b (min)	t_s (min)	Q_b (sccm)	Q_c (slm)	Q_h (sccm)
300	775	1	30	85	1.3	115

Table 2.1 - Parameters for optimal water-assisted CVD growth.

a



b

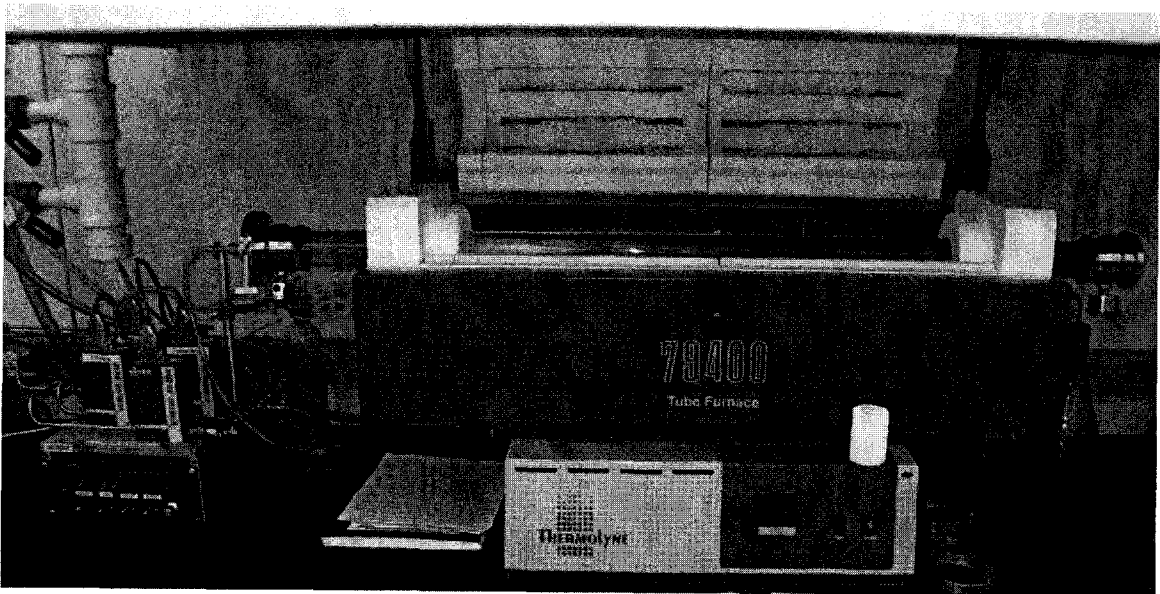


Figure 2.3 – Schematic (a) and photograph (b) of the pre-deposited catalyst CVD system.

Using the above procedure, the next step was to optimize the growth parameters. Despite the fact that this particular furnace was the one used to grow the DWNTs in reference [37], it had since been moved and had been reassembled with the new MFCs. Again, due to the sensitivity of the growth process, any small change in the growth environment may produce a large change in the success of the synthesis. As observed in the early growth runs, it was determined that the bubbling flow rate had the most significant effect on the success of the synthesis as compared to the temperature and flow rates of the other gases, and should be the main focus of the optimization work. Basing off of the previously successful growth parameters and the observations from the tests stated above, the parameters in Table 2.1 (with the obvious exception of Q_b) were selected to optimize this parameter; a series of growth runs with various flow rates through the water bubbler were conducted, and the resulting heights of the growths (as measured by SEM) were compared. In Figure 2.4, we can see that from 0 – 125 sccm of flow through the bubbler, ~85 sccm appears to be the flow rate by which to pick up the optimum amount of water vapor to promote the tallest growth given the other parameters. With these parameters, growths up to 2.5 mm in-length were achieved with consistent repeatability.

2.1.3. A-CNTs Grown Via Pre-Deposited Catalyst CVD

By using the previously-mentioned parameters, I was able to synthesize even, regular mats of aligned CNTs with fairly high repeatability. Examples can be

seen in the images in Figure 2.5, where we can also see that the CNTs all have approximately the same diameter.

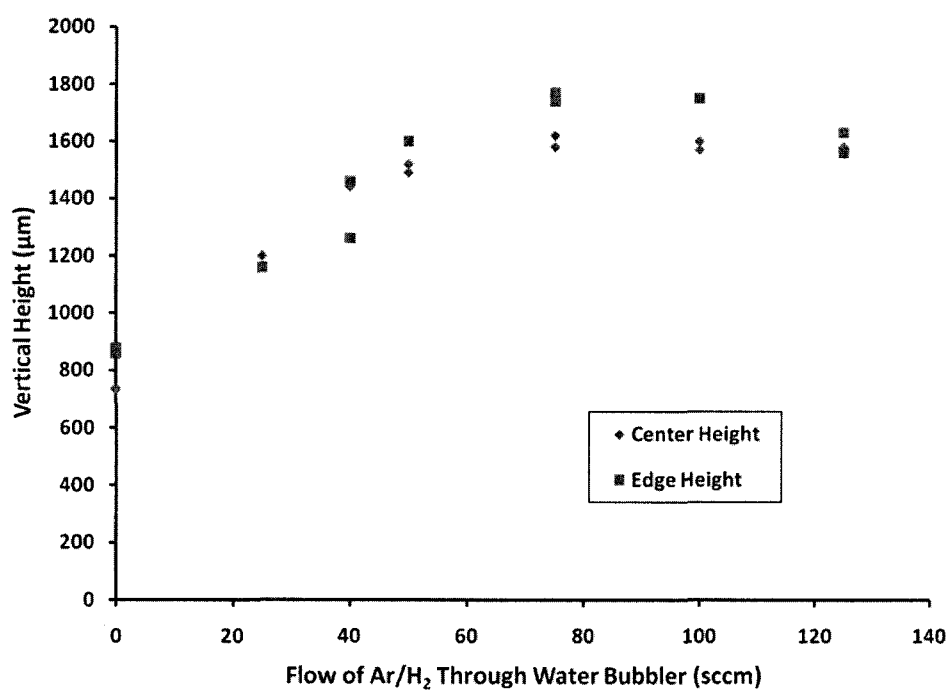


Figure 2.4 – Growth height as a function of water vapor content.

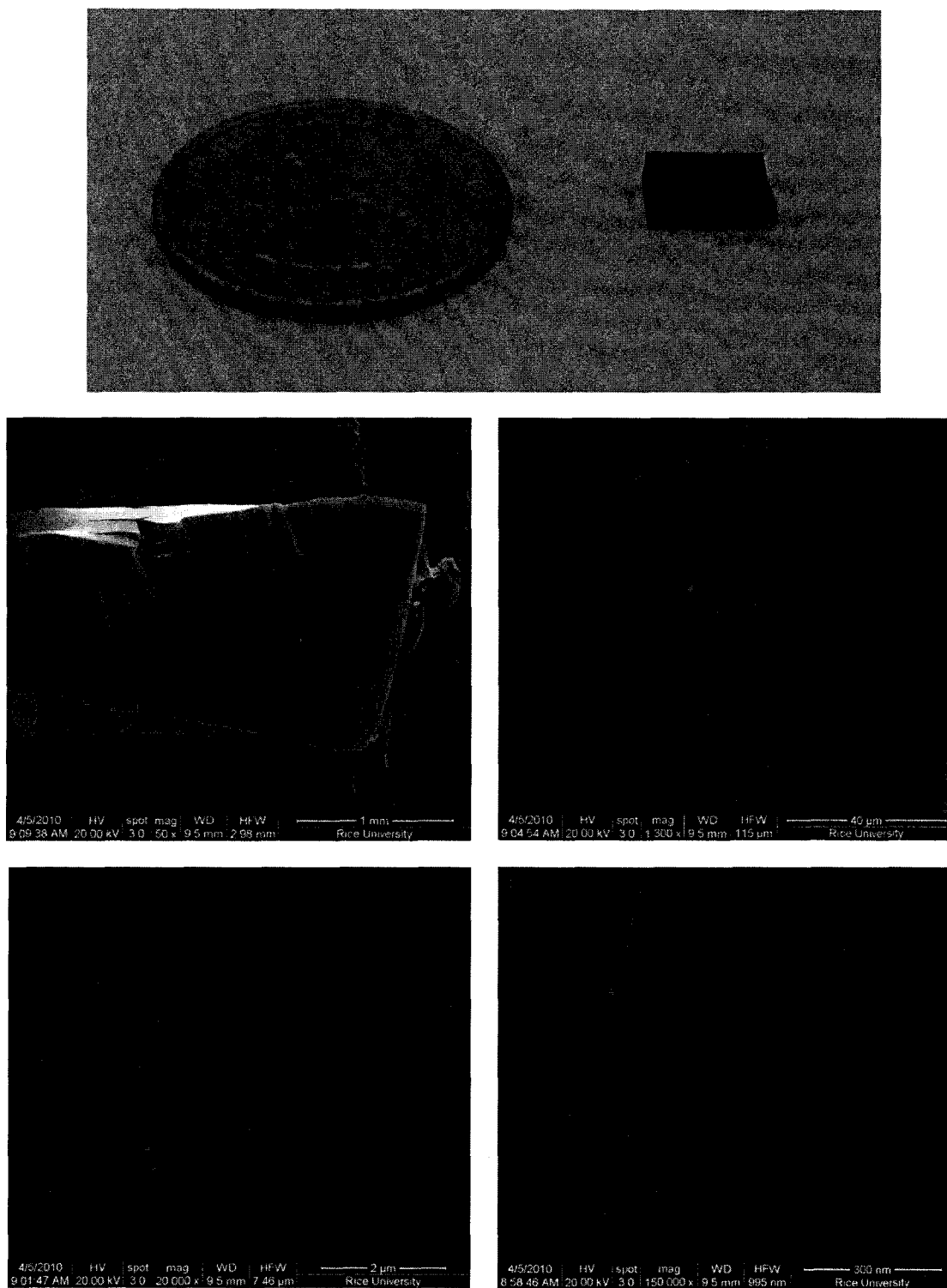


Figure 2.5 – Water-Assisted Pre-Deposited Catalyst CNTs.

2.2. Vapor-Phase CVD

2.2.1. Introduction to Vapor-Phase CVD Growth

As compared to the pre-deposited catalyst method, the vapor-phase CVD process allows for the growth of CNTs on much more complex surfaces. In this technique, the catalyst precursor is dissolved in an organic solvent and introduced with the carbon feedstock through liquid delivery. As the solution evaporates and the dissociated precursors pass through the system, the catalyst particles will land on surfaces in the reaction chamber, where the carbon will interact with them to initiate the growth of a CNT. This opens up the possibility for CNT growth on surfaces which are more complex or otherwise are not suitable for the pre-deposition of a catalyst. It has been shown that CNTs can be readily grown on many surfaces, ranging from oxidized silicon to quartz and even on the surfaces of carbon fibers via this method [38]. Similarly to pre-deposited catalyst CVD, it is also possible to pattern the growth of CNTs through vapor-phase CVD. By patterning an oxide layer on a silicon substrate, it has been shown that CNTs will only grow on the oxide, allowing for the selective growth of 2D and even 3D patterns such as pillars and “daisies” [39].

While it may be considered a downfall for most applications, the CNTs grown via vapor-phase CVD tend to be of a lower quality, due in part to the fact that the amount of catalyst is not nearly as well-controlled. This tends to result in CNTs which have varied diameters and are not nearly as crystalline (at least for the outer coaxial layers) and may also have an amorphous or pyrolyzed carbon coating. The

water-assisted pre-deposited catalyst CNTs synthesized via our method are predominantly DWNTs and FWNTs, whereas the vapor-phase CVD growth largely results in MWNTs which have much larger diameters (up to 100+ nm). For composite applications, the percent crystallinity is not as great of a concern when working with MWNTs, as a defective surface may allow for a greater interaction with the matrix through surface roughness or perhaps covalent interaction (via any dangling bonds on the CNT surface). Moreover, the multiple layer structure of MWNTs already improves their mechanical strength as compared to lesser-walled CNTs.

2.2.2. Construction of a Vapor-Phase A-CNT Growth Furnace

As with a pre-deposited catalyst CVD system, a stable, high-temperature growth region is necessary for vapor-phase CVD. For the purposes of this work, a Lindberg/Blue M 55347 three-zone tube furnace was used to ensure the longest growth zone. The benefit of a three-zone furnace lies in the ability to extend the length of the central zone to prevent temperature drops on the ends of the center zone. By increasing the temperature on the end zones by 5-10 °C as compared to the central zone, the width of the isothermal central zone is extended, ensuring the longest-possible region for consistent CNT growth. For the growth runs executed for this work, the end zones were heated 8 °C higher than the center zone and the furnace is 35" in-length, allowing for a very large zone for CNT synthesis. This furnace can accommodate a 3" processing tube, and custom 8' quartz tubes were

ordered in order to ensure that the flanges capping the ends did not heat up during synthesis.

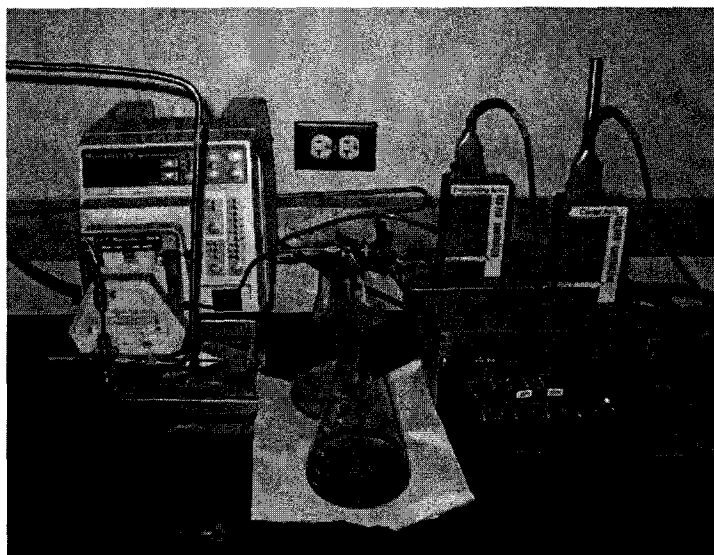


Figure 2.6 – Continuous pump, xylene/ferrocene mixture, and mass flow controllers for vapor-phase CVD.

As the carbon/catalyst precursors are not gaseous for this method, they need to be introduced to the system in the liquid state, which necessitates a more complicated delivery system. Previous methods of liquid delivery include injection [40], spray [41], and aerosol [42], though these methods all necessitate either a secondary heater or other hardware to prepare the mixture for introduction to the reaction zone. For this work, the catalyst/carbon source mixture used was ferrocene dissolved in xylene, and with xylene's boiling point being 139 °C, the mixture must be heated up to this temperature before it can mix with the buffer gases to pass through the reaction zone.

To simplify the experimental setup and eliminate the need for a secondary heating source, a novel method by which to utilize the residual heat of the end of the furnace in order to evaporate the mixture was designed. By pumping the mixture using a Masterflex 7523 continuous pump to near the edge of the furnace, the waste heat from the furnace is sufficient to evaporate the xylene/ferrocene mixture so that it can be carried in the gaseous phase through the reaction zone. In order to ensure even and consistent dispersion of the growth precursors, two gases, also controlled by MKS M100 MFCs controlled by a MKS Type 247 Four-Channel Readout were used: the “evaporator gas” (15 vol% hydrogen, balance argon) is to help the evaporated xylene/ferrocene mixture to be evenly dispersed, and the “carrier gas” (15 vol% hydrogen, balance argon) was used to carry the precursors/evaporator gas mixture through the furnace. An image showing the pump and the MFC bank can be seen in Figure 2.6.

As can be seen in Figure 2.7, the carrier and evaporator gases are directed through coaxial channels which surround the precursor mixture, all of which are made of stainless steel tubing and measure 1”, $\frac{1}{4}$ ”, $\frac{1}{16}$ ” in-diameter, respectively. The carrier gas line ends at the flange of the quartz tube, where it will result in an even flow which downstream will pick up the reaction gases and carry them towards the reaction zone. The evaporator gas line is supported by the rigidity of the $\frac{1}{4}$ ” tube, where it will carry the gas to the “evaporator”, a custom-fabricated part which creates an environment where the evaporated catalyst/carbon source can disperse with the evaporator gas before being sprayed radially into the quartz

tube where it will be picked up by the carrier gas and carried through the reaction zone. The entire vapor-phase CVD growth setup is pictured in Figure 2.8.

With the furnace assembled, again comes the task of developing a successful growth method. The parameters used for the successful synthesis of A-CNTs via the xylene/ferrocene process [43] were used as a starting point for this setup, and the procedure used for the synthesis of these CNTs is as follows:

1. Begin flowing the carrier gas (Q_c) and heat furnace up to the introduction temperature (T_i).
2. When stable, place substrate into the center of the growth zone and begin heating to the desired set point temperature for the synthesis (T_s).
3. At the exact time the set point is reached, begin flow of evaporator gas (Q_e) and initiate the flow of the catalyst/carbon source liquid mixture (Q_ℓ) which has a specific ratio of catalyst-to-carbon-source (C:CS).
4. After the desired synthesis time (t_s) has elapsed, turn off all flow but the Q_e during cool down.

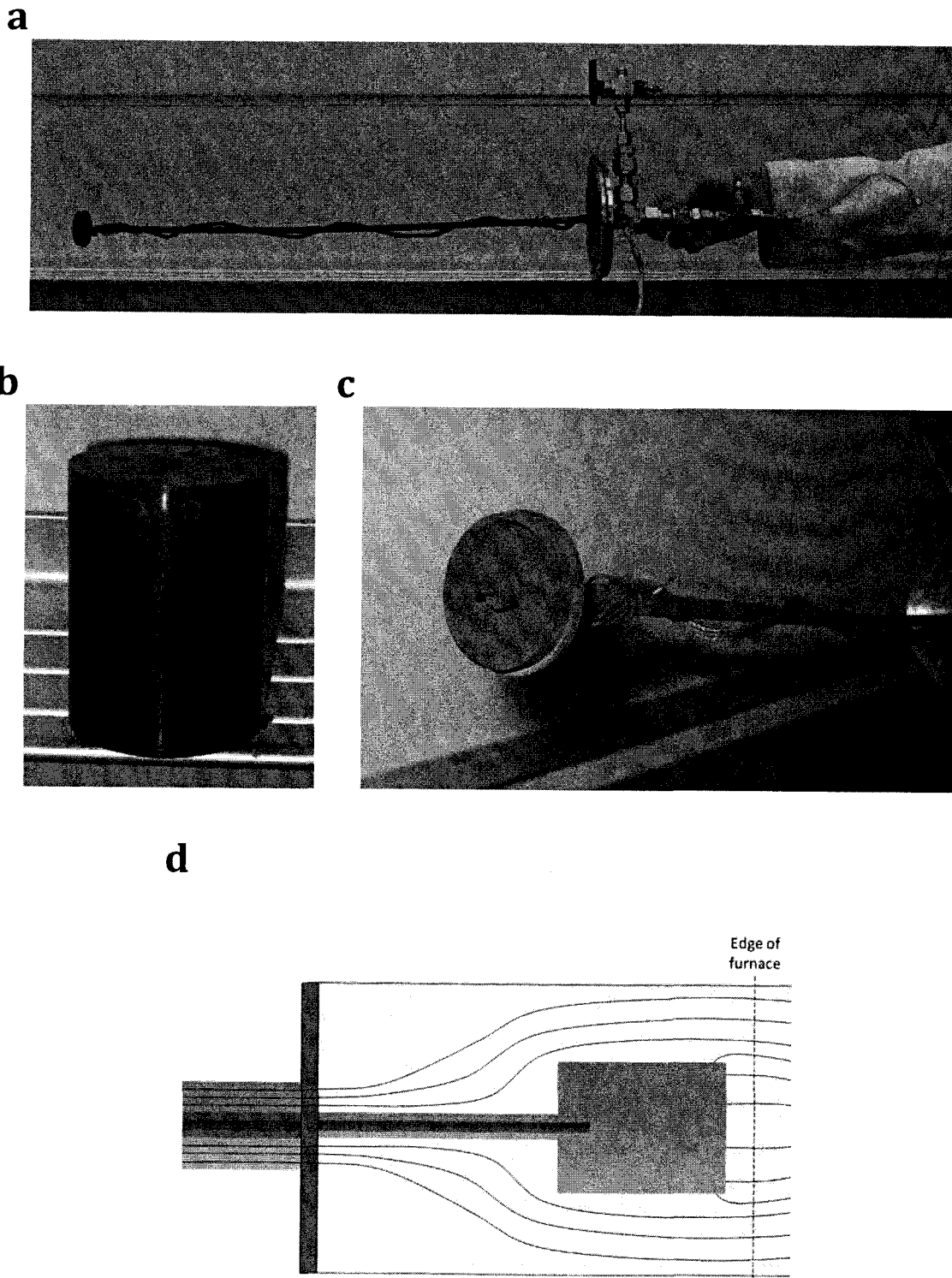


Figure 2.7 – Photographs of the coaxial gas/liquid delivery (a), evaporator cap (b) and its seat (c), and schematic of gas flow around evaporator (d).

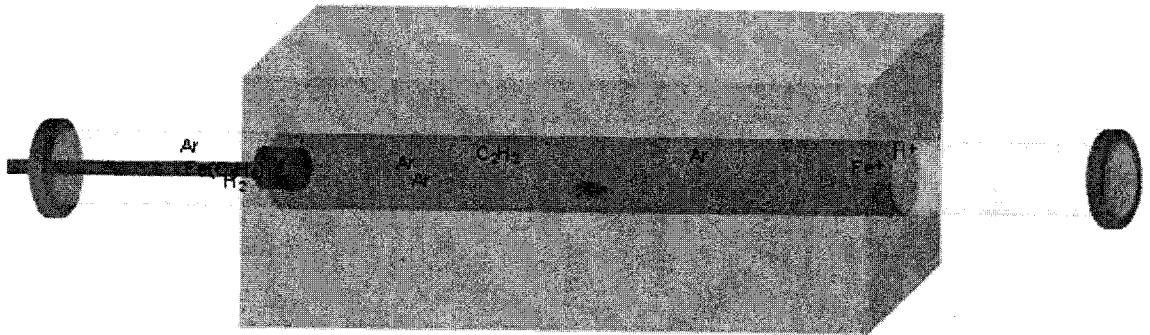
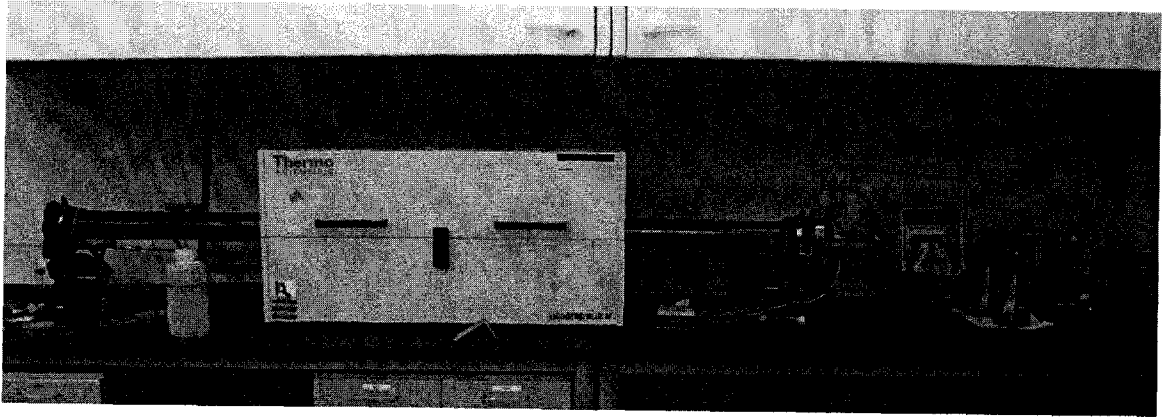
a**b**

Figure 2.8 – Schematic (a) and image (b) of the vapor-phase CVD system.

2.2.3. A-CNTs Grown via Vapor-Phase CVD

In contrast to what was observed with the pre-deposited catalyst CVD technique, longer growths of A-CNTs are possible through vapor-phase CVD, and it has been shown that CNTs can be grown in excess of 1 cm in-length through this process [43]. Due to the added complexity of the vapor-phase delivery method, the reaction parameters can become more difficult to optimize, making it harder to produce higher-quality CNTs. The added degree of freedom with having to actively control the catalyst content not only makes growth optimization more time-consuming, but also will inherently result in CNTs with more metal content. However, if the embedded metal content of the CNTs is not of concern, the act of constantly adding more catalyst to the system during synthesis via this process can help stave off catalyst death and allow for longer A-CNTs. Another downfall of this technique is that the CNTs tend to not be uniform in diameter. As depicted in Figure 2.9, the “top” of the CNTs are considerably thicker than the “middle”, and especially the “bottom”.

T_i (°C)	T_s (°C)	t_s (min)	C:CS ($\frac{\text{mg}}{\text{ml}}$)	Q_e (sccm)	Q_c (slm)	Q_f ($\frac{\text{ml}}{\text{min}}$)
300	775	300	.2	500	1	.2

Table 2.2 – Parameters for vapor-phase CVD growth.

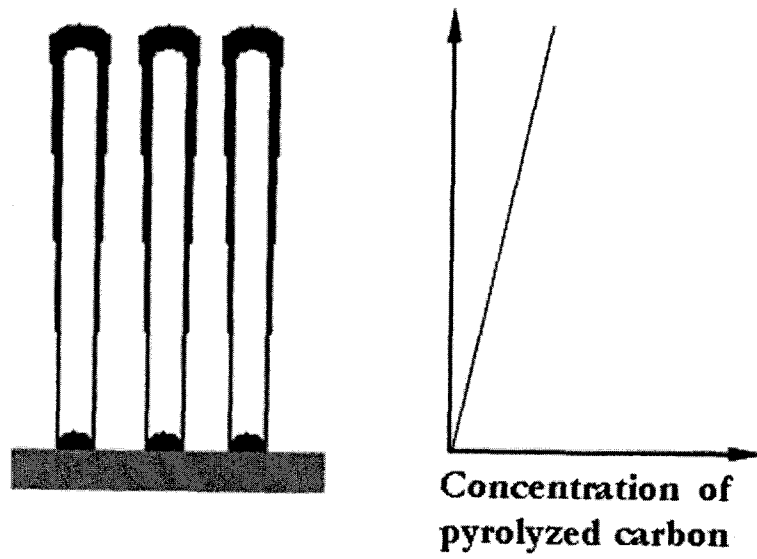


Figure 2.9 – Schematic of vapor-phase CNT thickness as a function of growth height [44].

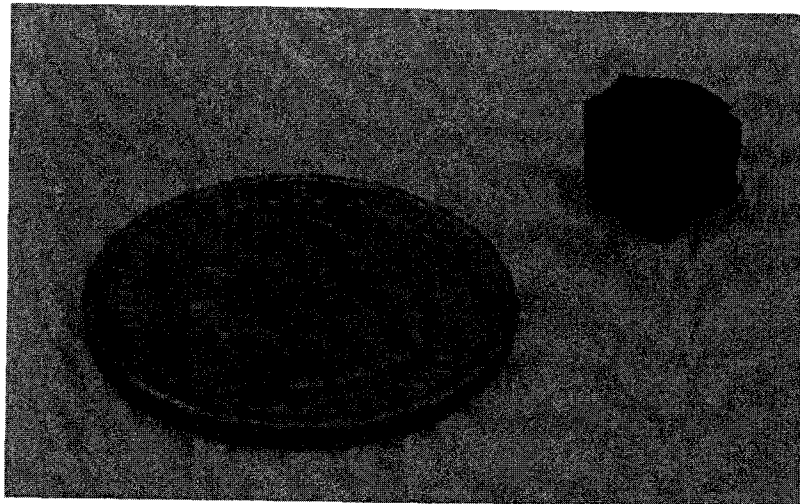


Figure 2.10 – Photograph of A-CNTs grown via vapor-phase CVD.

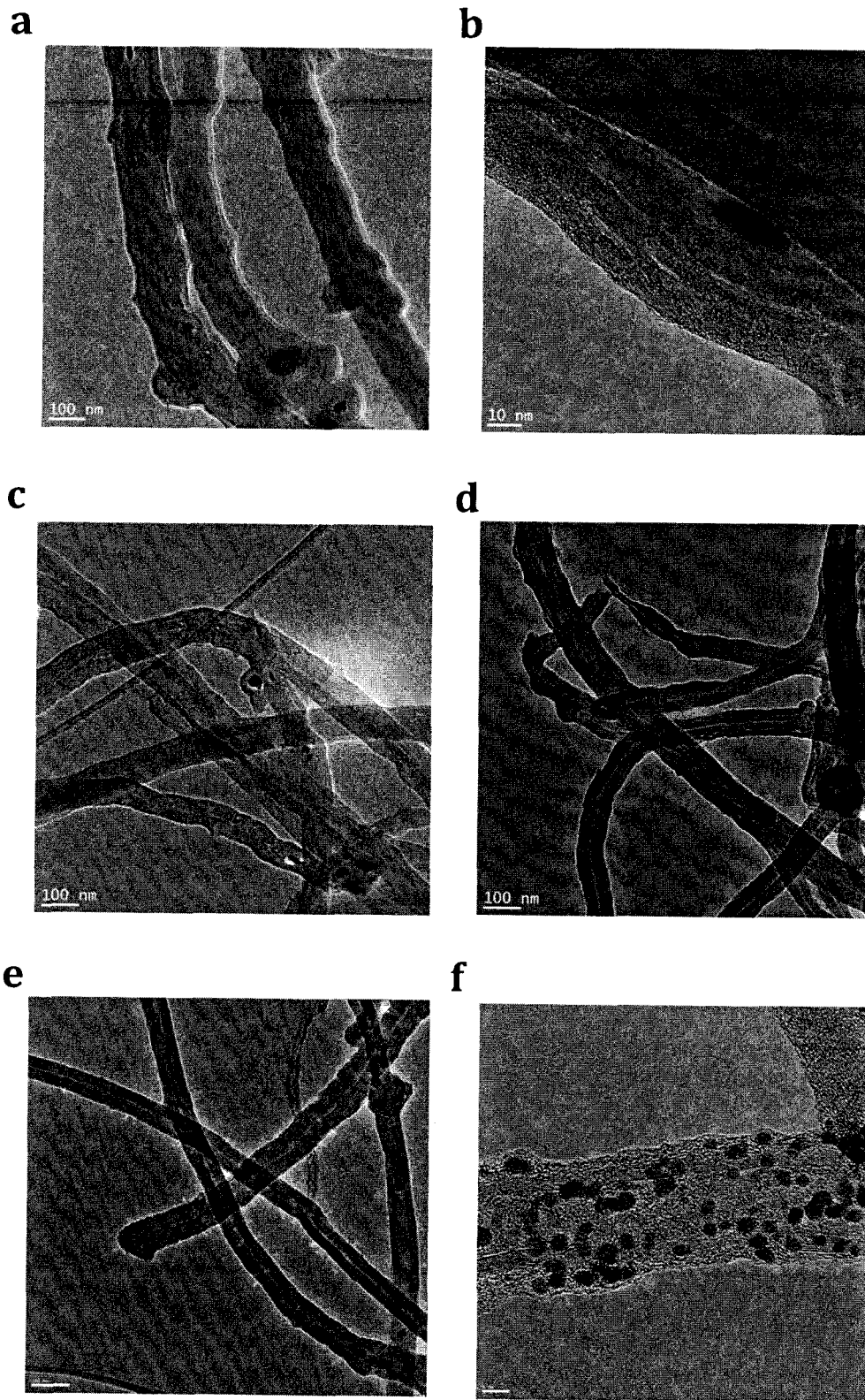


Figure 2.11 – TEM images of the “top” (a,b), “middle” (c,d), and “bottom” (e,f) of xylene/ferrocene A-CNTs.

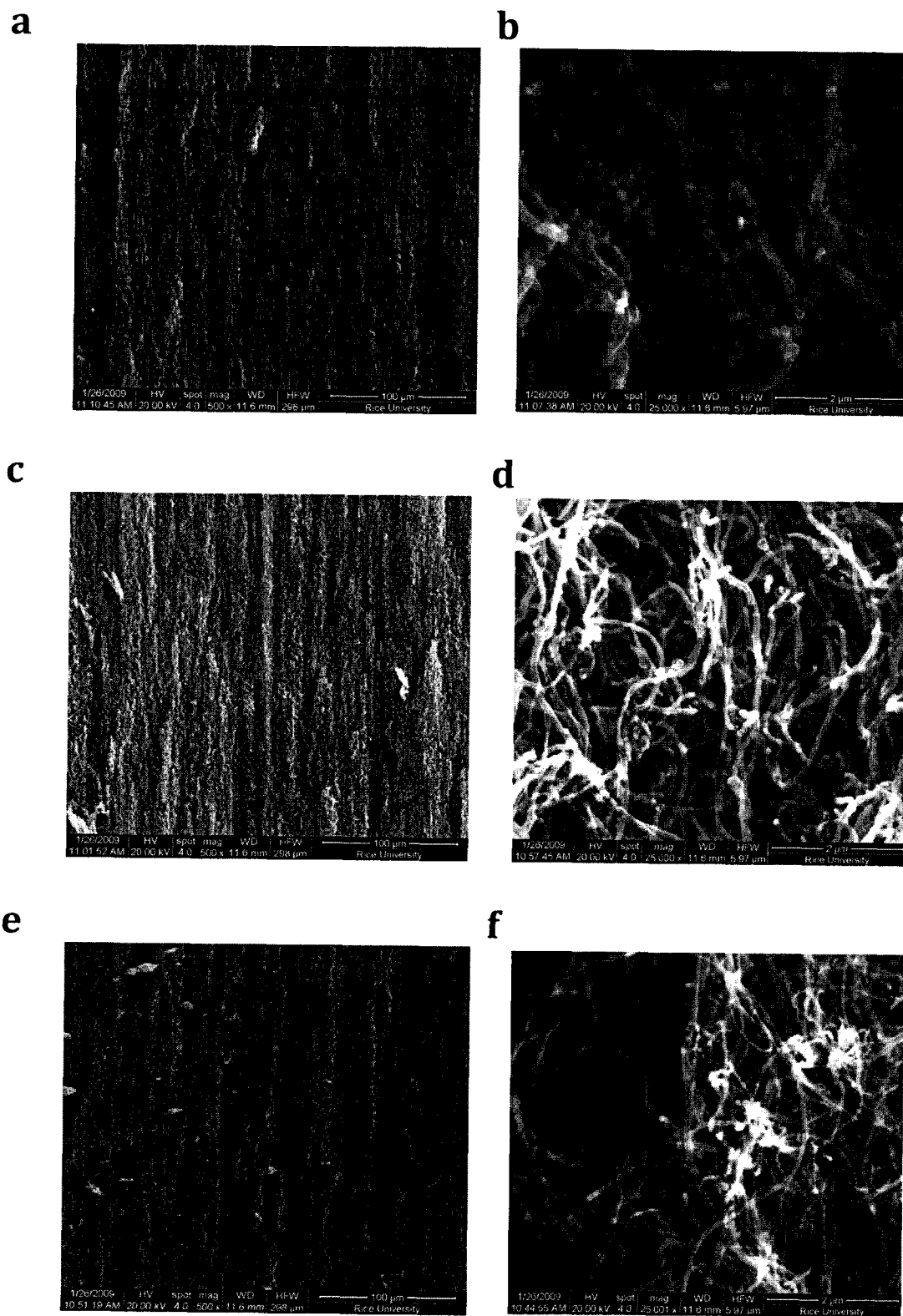


Figure 2.12 – SEM images of the “top” (a,b), “middle” (c,d), and “bottom” (e,f) of xylene/ferrocene A-CNTs.

Based on previously-reported parameters for similar synthesis, the parameters in Table 2.2 were selected for the growth of the A-CNTs for this study. A representative sample of the A-CNTs grown is displayed in Figure 2.10, where it can be seen that the CNTs are considerably taller than those grown via pre-deposited catalyst CVD. TEM images of these CNTs (Figure 2.11) reinforce this and also clearly show that the CNTs, while not perfectly crystalline, are graphitic in the outer layers. The coating at the “bottom” of the CNTs is much thinner, indicating less pyrolyzed/amorphous carbon since this region of the CNT was synthesized only shortly before the growth terminated, and the large spots are iron nanoparticles which are embedded in the walls of the CNTs. In the SEM images of these three regions in Figure 2.12, we also observe that the alignment of the “top” of the CNTs is much more anisotropic as compared to the “bottom”, where two mechanisms may be contributing to a loss of general alignment; these methods include: 1) the weight of the thicker CNTs may be inhibiting the alignment, causing more “waviness” in the CNTs, and 2) the constant injection of fresh catalyst is causing “new” CNTs to grow, which are not growing normal to the substrate, causing additional isotropicity of the CNTs in this region.

2.3. Comparison of A-CNTs for Infiltrated Composite Applications

The first comparison that can be made between the CNTs grown by these two different methods is the lengths that can be grown. The pre-deposited CVD technique used here has not been reported as being able to grow CNTs much longer than the 2.5 mm forests grown for this study. When growing A-CNTs for composite

applications, clearly longer-length CNTs are ideal as it makes it possible to produce much thicker continuously-reinforced composites.

Additionally, the surface roughness should play a role in the efficiency of load transfer from the matrix to the CNTs, thereby improving the overall bulk properties. Efficient load transfer is an issue which has plagued nanocomposites since their inception, and it has been suggested that interfacial strength can be improved through non-covalent interactions such as polymer wrapping and covalent bonding through the functionalization of the CNT surface [45]. Furthermore, the MWNTs produced through the vapor-phase CVD process are more ideal as reinforcement in polymer composites due to their higher stiffness as compared to the thin-walled CNTs produced through the pre-deposited catalyst CVD method.

In the next chapter, I will specifically discuss the drawbacks and successes of each type of A-CNT forest for the purposes of developing successfully-infiltrated composites, and will explore their fundamental dynamic mechanical behavior.

Vertically-Aligned Carbon Nanotube/ Poly(dimethylsiloxane) Composites

With the A-CNT forests grown, the next task is to utilize them as the reinforcing phase of a composite and to use dynamic mechanical analysis (DMA) to discern their mechanical properties. As these composites are not mixed, the ability of the desired matrix to infiltrate the A-CNT forest is critical for success; this infiltration is highly-dependent on the wetting (contact angle) between the CNTs and the matrix polymer. The wetting behavior between the CNTs and the desired matrix is important for the success of a composite, as it ultimately dispersed and matrix phases. The wetting between CNTs and many polymers has been explored [35], and a few of these polymers have been recently explored as an infiltrating matrix for A-CNT composites [34],[46].

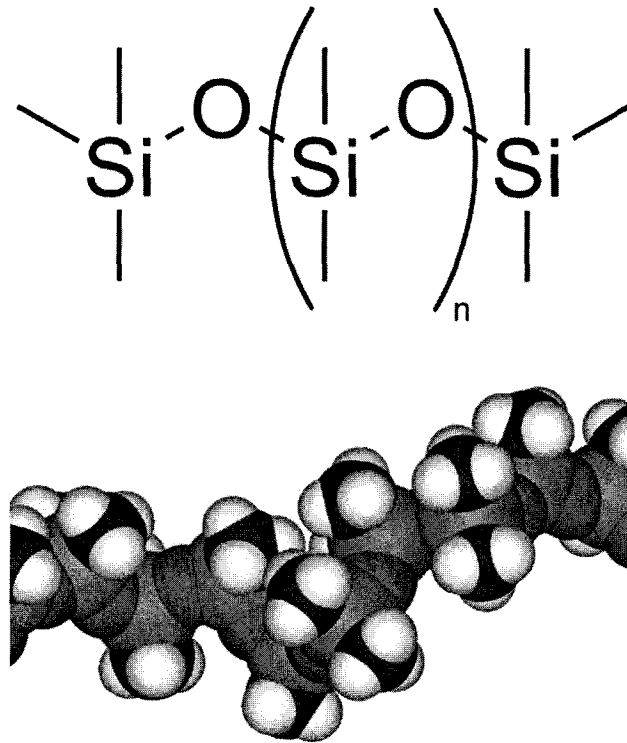


Figure 3.1 - Molecular structure of PDMS [47].

3.1. Introduction to Poly(dimethylsiloxane)

PDMS is an optically-clear silicone elastomer with a molecular structure as shown in Figure 3.1. The silicon-rich backbone results in very flexible polymer chains which can easily slip past each other. The loose entanglement of these chains provides PDMS with very prominent viscoelastic features, properties which can be tuned by the molecular weight of the polymer chains. It is a chemically stable and biocompatible polymer [48] with a poisson ratio of ,5, and is commonly used in many diverse applications ranging from silicone caulks and lubricants to cosmetics

and even hair care products [47]. Its unusual flow properties also allow it to conform to very small features if allowed to flow for an extended period, and as such, commercial PDMS compounds have seen much success in the field of microfluidics [49]. For the current work, the PDMS used was Sylgard 184, as provided by Dow Corning, which comes in a two-part mixture which includes the PDMS monomer and a curing agent which induces the PDMS chains to covalently link together and form a highly-compliant solid.

Poly(dimethylsiloxane) (PDMS) was selected as the matrix for these composites due to its extremely high wetting of CNTs [35], in addition to the fact that it is commercially available and easy to work with. As with other elastomers, PDMS is very elastic and extremely compliant at room temperature. To achieve large-amplitude strains, the testing needs to be conducted while the polymer is in the “rubbery” state, so choosing a matrix with a very low glass transition (T_g) such as PDMS (-129 °C) is ideal.

3.2. Composite Preparation

The infiltration technique used was very similar to the method used in the paper which introduced these continuously-aligned CNT-reinforced composites [46]. A detailed procedure is as follows:

1. Mix the PDMS monomer and the curing agent at a 10:1 ratio and stir for 5 minutes to ensure homogeneity.

2. Place the pre-cured polymer under house vacuum in order to remove any interstitial air. Remove when bubbling has ceased (~ 10 minutes).
3. Introduce a free-standing mat of A-CNTs by placing it on top of the pre-cure, and “scoop” some of the polymer onto the top of the forest to promote infiltration.
4. After fully submerged, place the infiltrating composite under a vacuum of 1 Torr for at least 3 hours until bubbling has ceased.
5. When no longer bubbling, subject the sample to 1 hour of 100 °C heat treatment as recommended by the manufacturer to ensure complete curing.

This preparation technique was used for both types of A-CNTs grown via the previously-mentioned CVD techniques. The next sections will address the results from these attempts in creating A-CNT composites.

3.2.1. Results from Pre-Deposited Catalyst A-CNT Infiltration

As mentioned previously, the pre-deposited catalyst A-CNTs are predominantly thin-walled CNTs, with the majority being DWNTs. After numerous attempts at infiltration, it was repeatedly observed that these relatively flimsy CNT forests were not able to maintain their alignment during infiltration, and would “crumple” as the polymer infiltrated. As the curing agent is dispersed in the monomer prior to infiltration, there is a finite time where the polymer will have the fluidity to infiltrate the forest before it becomes too viscous and eventually solidifies due to the crosslinking. Coupled with the high viscosity of the Sylgard 184 monomer, successful infiltration of these relatively delicate forests seems

improbable without disturbing their alignment. In Figure 3.2, it is easy to see that these pre-deposited catalyst CNTs buckled quite significantly during the infiltration as observed by the wavy structure of the fractured surface.

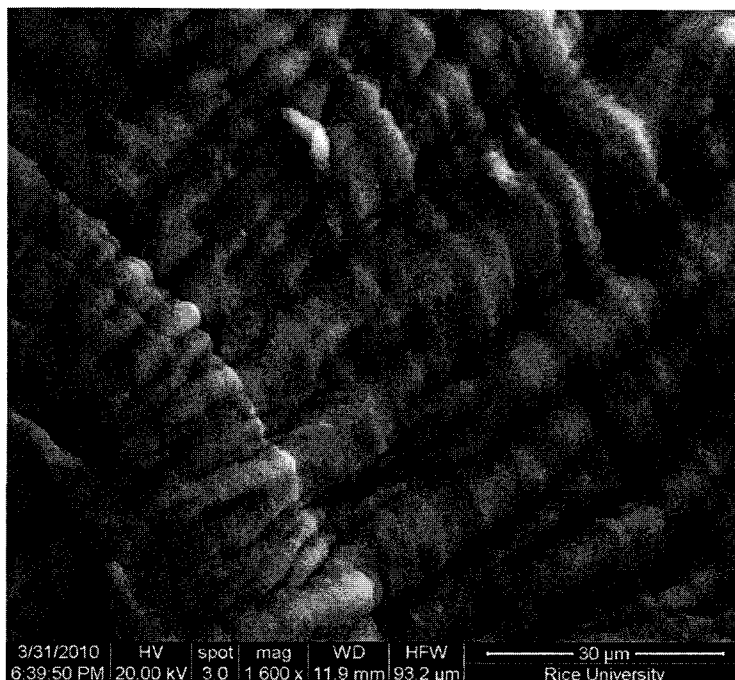


Figure 3.2 – SEM image of poor alignment in pre-deposited catalyst composite.

3.2.2. Results from Vapor-Phase A-CNT Infiltration

The vapor-phase-grown A-CNTs were much more successful during the infiltration of PDMS. Due to their much larger diameter and slightly higher entanglement, it was easier to infiltrate these A-CNTs without disturbing the existing organization of the CNTs. In Figure 3.3 it can be seen that not only is there good interface between the CNTs and the polymer, but that in these composites, the CNTs have retained their alignment. The successful infiltration of these CNTs

qualifies these composites for further analysis, which for this thesis work includes the analysis of their responses to various levels of dynamic mechanical stress.

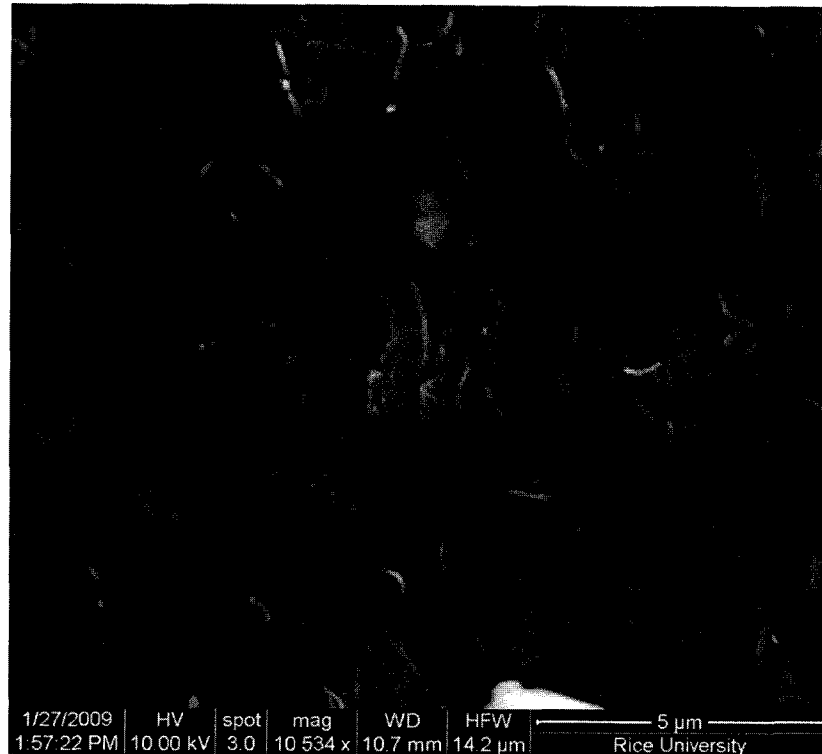


Figure 3.3 – SEM image of the good polymer/CNT physical interaction and CNT alignment for vapor-phase A-CNT/PDMS composites.

3.3. Dynamic Mechanical Properties of A-CNT/PDMS Composites

DMA is an incredibly powerful technique for the analysis of materials, and particularly for polymers. By subjecting a material to an oscillating mechanical strain, information regarding the viscoelastic properties such as the storage (E') and loss (E'') moduli and damping ($\tan \delta$) can be determined. Tight control over the amplitude and frequency of oscillation and the ambient temperature makes it

possible to reveal very specific thermomechanical information about a material, ranging from basic stress-strain behavior to subtle thermal transitions which occur in the polymer and may be very difficult if at all possible to observe through microscopy or spectroscopy.

Due to the height limitations of the available A-CNTs which can be grown, compression remains the only viable method for this type of testing. The high compliancy of PDMS allows for the compression of these composites to high strains dynamically, making DMA relatively straightforward, as explained in Figure 3.4. Another benefit of using PDMS is the ease of sample preparation. PDMS can be very easily cut by using a razor blade and a steady hand, and for all of the following data, samples measuring 2.5 mm long x 1 mm wide x 1 mm tall were used. Due to the anisotropy of the CNTs in these samples, they can be tested in two particular orientations: 1) longitudinal to the alignment of the CNTs (axial), or 2) transverse to the alignment of the CNTs (radial); a schematic of the particular orientations as compared to the neat polymer and a SEM image of a sample can be seen in Figure 3.5.

Over the next few sections, I will discuss the fundamental dynamic mechanical properties as observed through DMA, and the information revealed by these tests as compared to the properties of the neat polymer.

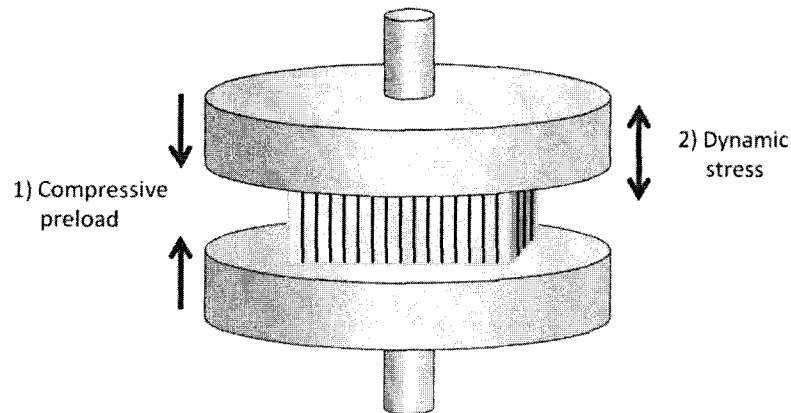


Figure 3.4 – Schematic of axial dynamic compression on the A-CNT composites.

3.3.1. Strain Sweep

Typically the first test done when conducting DMA, the strain sweep will reveal the strain-dependent response of a material. This is done by choosing a constant frequency and temperature and then applying a stable oscillating strain to the sample. The viscoelastic response of the material at that strain is recorded, and the instrument will continue on to the next strain. A strain sweep is essential as it will reveal the linear region of deformation for a sample, which is the region where further dynamic testing should be conducted in order to assuredly obtain meaningful data. The data presented in this section is conducted at room temperature and at a frequency of .5 Hz.

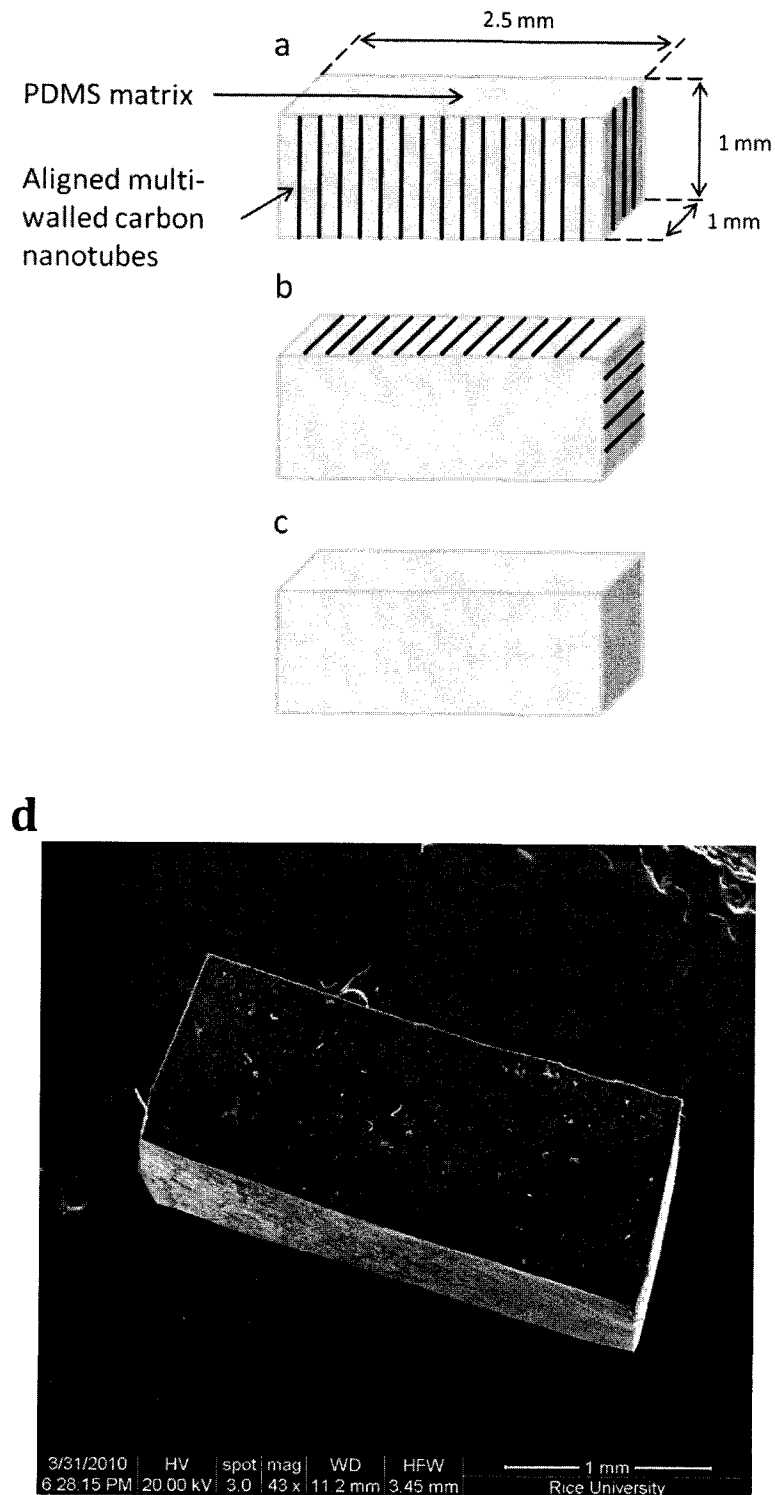


Figure 3.5 – Schematic of the axial (a), radial (b), and neat polymer (c) samples, and a SEM image (d) of the samples used for DMA testing.

In Figure 3.6 the strain sweep data for the bottom composite is presented for a .5 Hz, room temperature test. When tested radially, aside from the obvious observation that the storage and loss of the composites is approximately 4- to 5-fold greater than the neat polymer, interestingly the composites do not displace nearly as much as the neat PDMS before reaching the final stage of elastomer deformation. The mechanism of elastomers' high elasticity lies in the ability for the polymer chains to elongate under stress. At the point where its polymer backbones are fully stretched, an elastomer will resist further deformation and its properties will spike rapidly. There are two likely explanations for the decreased strain limit for the composites: 1) at this strain the polymer may largely have been pushed out from in-between the CNTs, which would promote much more CNT-CNT physical interaction, and/or 2) the entanglement of the chains around the CNTs may reduce their mobility and result in the full elongation of those chains at lower strains. The first mechanism is fairly self-explanatory, but the second can be rationalized through the mechanism by which the polymer infiltrates the forest of CNTs. The polymer chains work their way between the A-CNTs from all directions and at differing rates. As such, the entanglement of the polymer chains around the CNTs is most likely very high. As the composites are stressed and the chains begin to elongate to accommodate that strain, entanglement around the CNTs will inhibit displacement to strains which are normally achievable for the neat polymer.

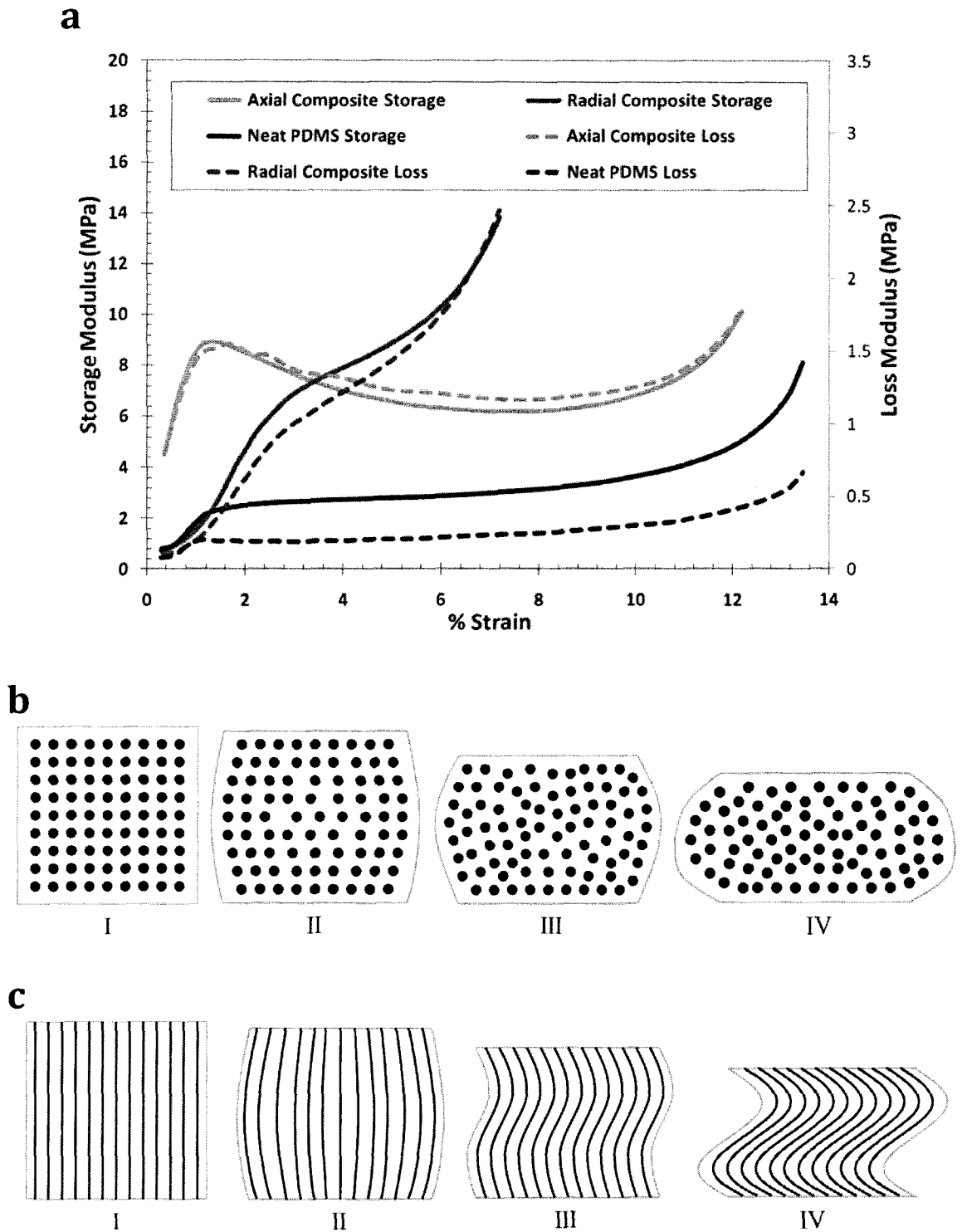


Figure 3.6 – Storage and loss moduli (a) of a strain sweep DMA test. Schematics showing the radial (c) and axial (d) displacement of the CNTs under strain.

Axial testing reveals a trend which differs greatly from that of the neat polymer and the radial testing. There is an obvious peaking of the storage and loss above a 1% strain amplitude, which is explained by the buckling of the CNTs within the composite. This peaked strain amplitude is the critical threshold where the composite transitions from a “bulging” compression to an “S-shaped” global buckling of the CNTs.

Furthermore, it is curious that in contrast to the radial testing, the composites have a maximum displacement similar to that of the neat polymer. A likely explanation for this is that by buckling, the CNTs are preventing the sample from bulging during compression. The bulging of the sample causes the polymer chains to become fully-extended at lower strains, hence the lower maximum displacement. During axial compression, there is much less chain stretching normal to the direction of deformation, allowing the composite to compress to nearly the same displacement as the neat polymer.

3.3.2. Frequency Sweep

For a particular strain amplitude and temperature, a frequency sweep will resolve any frequency-dependent behavior for a given sample. With consideration given to any dependencies due to the dimensions of the sample, particular interactions which may occur in a sample will be elucidated through this type of testing. The frequency-dependent testing presented in this thesis is a result of testing the bottom CNTs and was conducted at room temperature and at a strain amplitude of 1%, as determined from the observation from the strain sweep testing

that there is no linear region of elastic deformation for these samples above this value.

As displayed in Figure 3.7, the composites respond almost identically to the neat polymer with the exception of two particular frequency ranges: 1) 57-70 Hz for the radial test, and 2) 75-95 Hz for the axial test; frequency range #1 indicates a significant spike in damping for the radial test, while frequency range #2 shows a relatively similar enhancement for the axial test. An explanation for this behavior is that at these frequencies, the samples were in resonance in the direction of the CNT alignment. When in resonance along the length of the CNTs, greater interfacial friction is likely to occur, which could reasonably explain the notable enhancement in damping for those particular frequencies.

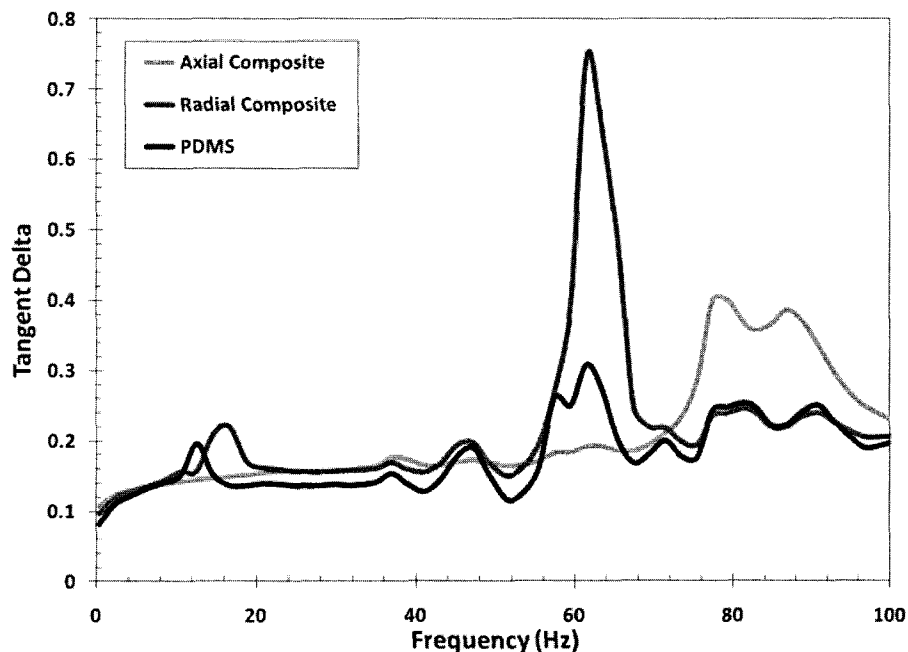


Figure 3.7 – Tangent delta for a frequency sweep DMA test.

3.3.3. Temperature Ramp

Varying the temperature for a constant frequency, constant strain test is perhaps the most powerful technique in DMA. Temperature-Dependent behavior can be used to observe subtle nuances in a polymer's structure, such as its cross-link density, degree of crystallinity, and thermal stability.

In Figure 3.8 we observe that for a 2 Hz, .3% strain amplitude test, there is no obvious difference in the glass transition between the composite and the neat polymer. The similarly-shaped and non-shifted tangent delta peak drives the conclusion that the structure of the polymer in the composite is similar to that of the neat polymer. The peak appears to be slightly lower than the neat polymer, which may indicate less amorphous content, but the shift is within error and, so far, inconclusive.

The point of thermal degradation tells a different story, as the composite shows much greater thermal stability. This polymer is rated to 200 °C, so it is not unexpected that the neat PDMS will show signs of degradation when heated past this temperature. However, it is clear that the composite is much less susceptible to such temperatures, indicating its superior thermal robustness. This resistance to failure may support the observation that CNTs may serve as radical scavengers [50], as the neutralization of any free radicals created above 200 °C would serve to preserve the mechanical integrity up until the temperature at which the polymer backbones begin to degrade. Otherwise, the introduction of free radicals will serve to initiate the escalating degradation of the polymer.

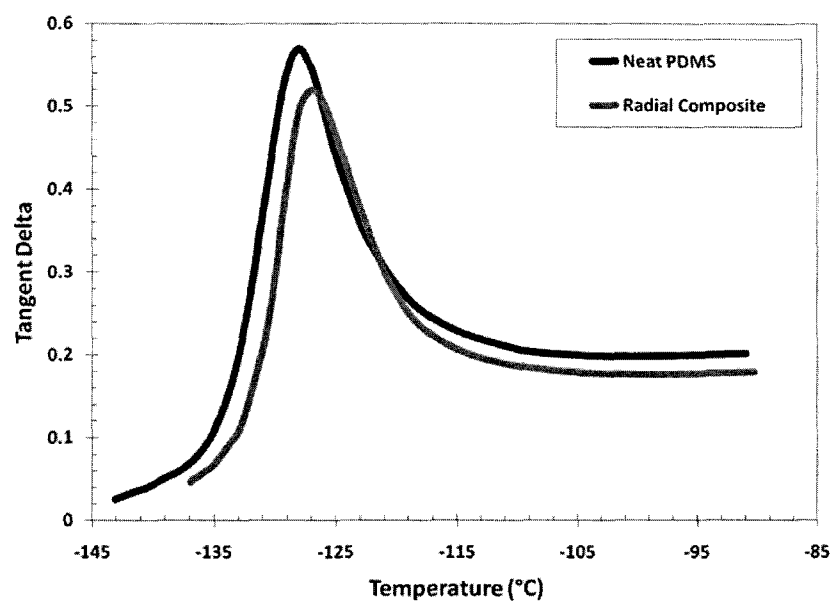
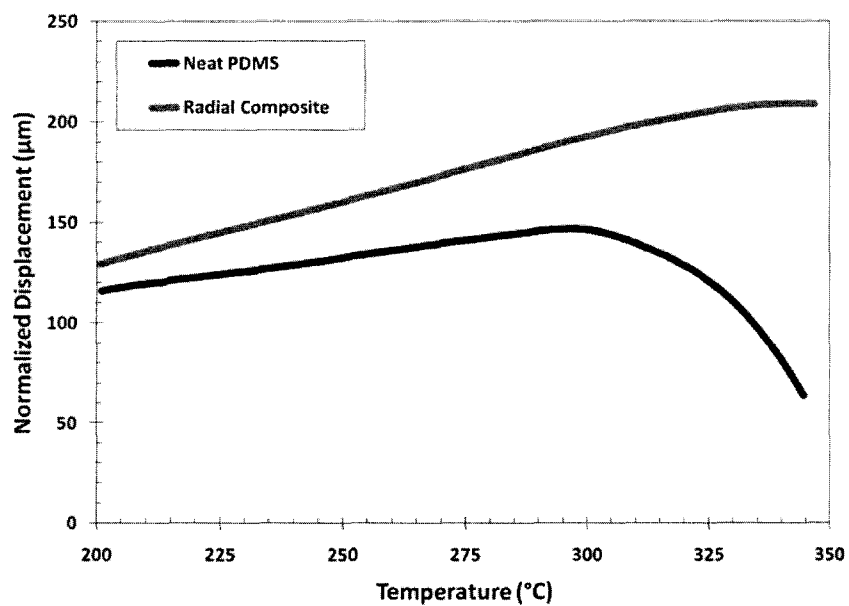
a**b**

Figure 3.8 – Temperature ramp showing the glass transition (a) and thermal degradation (b) of the composite vs. the neat polymer.

Conclusion and Future Work

There are many types and sizes of CNTs, and CVD has proven itself as a viable method for the large-scale production of CNTs for composite applications. Also produced via CVD, aligned CNTs help to solve many of the difficulties in the manufacturing of CNT-reinforced composites, which include agglomeration, non-homogeneous dispersion, and the alignment of the CNTs to maximize their contribution to the bulk properties of the composite. As these A-CNTs assemble into a self-aligned forest during synthesis, the CNT spacing is very regular, yet is sparse enough to allow for the infiltration of a polymer matrix.

While the quality of CNTs grown via pre-deposited catalyst CVD is generally much higher as compared to those grown via vapor-phase CVD, the DWNTs produced by this method simply cannot hold up to the force of the polymer infiltrating the free space between them. As a result, these thin-walled CNTs will buckle and lose their alignment during this process. Alternatively, the vapor-phase-

grown CNTs, with a greater rigidity and slightly higher entanglement, are robust enough to survive the force of a percolating polymer, making them a much more realistic option for mechanically-reinforced A-CNT composites.

Due to the compliancy of the PDMS matrix, these nanocomposites can be dynamically stressed to large strains, and such testing has revealed that these aligned CNTs in a composite matrix do impart not only significant improvement over the neat polymer, but their anisotropy can result in loading-specific responses. The thickness of the CNTs also plays a large role in their bulk properties, and axial loading has revealed that the storage is very high until a critical strain threshold, where the CNTs will enter a global buckling mode. Radial loading, however, largely mimics the trend of the neat polymer, though the yield strain is significantly lower due to polymer chain entanglement around the CNTs.

In addition to the further characterization of these composites, future work will include extended cyclic testing to determine the fatigue behavior of these polymer nanocomposites to gauge their viability in real world applications as mechanical reinforcement. Also, by understanding the high-cycle behavior of these materials, we can further shed light on the complicated interactions between these nanomaterials and polymer matrices.

References

- [1] S. Iijima, "Helical microtubules of graphitic carbon," *Nature*, vol. 354, Nov. 1991, pp. 56-58.
- [2] W.A. de Heer, A. Chatelain, and D. Ugarte, "A Carbon Nanotube Field-Emission Electron Source," *Science*, vol. 270, Nov. 1995, pp. 1179-1180.
- [3] C. Niu, E.K. Sichel, R. Hoch, D. Moy, and H. Tennent, "High power electrochemical capacitors based on carbon nanotube electrodes," *Applied Physics Letters*, vol. 70, 1997, p. 1480.
- [4] C. Liu, Y.Y. Fan, M. Liu, H.T. Cong, H.M. Cheng, and M.S. Dresselhaus, "Hydrogen Storage in Single-Walled Carbon Nanotubes at Room Temperature," *Science*, vol. 286, Nov. 1999, pp. 1127-1129.
- [5] E.S. Snow, F.K. Perkins, E.J. Houser, S.C. Badescu, and T.L. Reinecke, "Chemical Detection with a Single-Walled Carbon Nanotube Capacitor," *Science*, vol. 307, Mar. 2005, pp. 1942-1945.
- [6] K. Kordás, G. Tóth, P. Moilanen, M. Kumpumäki, J. Vähäkangas, A. Uusimäki, R. Vajtai, and P.M. Ajayan, "Chip cooling with integrated carbon nanotube microfin architectures," *Applied Physics Letters*, vol. 90, 2007, p. 123105.
- [7] Y. Shirai, A.J. Osgood, Y. Zhao, K.F. Kelly, and J.M. Tour, "Directional Control in Thermally Driven Single-Molecule Nanocars," *Nano Letters*, vol. 5, Nov. 2005, pp. 2330-2334.
- [8] S. Berber, Y. Kwon, and D. Tomanek, "Unusually High Thermal Conductivity of Carbon Nanotubes," *Physical Review Letters*, vol. 84, May. 2000, p. 4613.
- [9] C.T. White and T.N. Todorov, "Carbon nanotubes as long ballistic conductors," *Nature*, vol. 393, May. 1998, pp. 240-242.
- [10] M.M.J. Treacy, T.W. Ebbesen, and J.M. Gibson, "Exceptionally high Young's modulus observed for individual carbon nanotubes," *Nature*, vol. 381, Jun. 1996, pp. 678-680.
- [11] A.R. Harutyunyan, G. Chen, T.M. Paronyan, E.M. Pigos, O.A. Kuznetsov, K. Hewaparakrama, S.M. Kim, D. Zakharov, E.A. Stach, and G.U. Sumanasekera,

- "Preferential Growth of Single-Walled Carbon Nanotubes with Metallic Conductivity," *Science*, vol. 326, Oct. 2009, pp. 116-120.
- [12] T.W. Ebbesen and P.M. Ajayan, "Large-scale synthesis of carbon nanotubes," *Nature*, vol. 358, Jul. 1992, pp. 220-222.
- [13] M. José-Yacamán, M. Miki-Yoshida, L. Rendón, and J.G. Santiesteban, "Catalytic growth of carbon microtubules with fullerene structure," *Applied Physics Letters*, vol. 62, 1993, p. 202.
- [14] M. Endo, K. Takeuchi, S. Igarashi, K. Kobori, M. Shiraishi, and H.W. Kroto, "The production and structure of pyrolytic carbon nanotubes (PCNTs)," *Journal of Physics and Chemistry of Solids*, vol. 54, Dec. 1993, pp. 1841-1848.
- [15] P. Nikolaev, M.J. Bronikowski, R.K. Bradley, F. Rohmund, D.T. Colbert, K.A. Smith, and R.E. Smalley, "Gas-phase catalytic growth of single-walled carbon nanotubes from carbon monoxide," *Chemical Physics Letters*, vol. 313, Nov. 1999, pp. 91-97.
- [16] T. Guo, P. Nikolaev, A. Thess, D. Colbert, and R. Smalley, "Catalytic growth of single-walled nanotubes by laser vaporization," *Chemical Physics Letters*, vol. 243, Sep. 1995, pp. 49-54.
- [17] W.Z. Li, S.S. Xie, L.X. Qian, B.H. Chang, B.S. Zou, W.Y. Zhou, R.A. Zhao, and G. Wang, "Large-Scale Synthesis of Aligned Carbon Nanotubes," *Science*, vol. 274, Dec. 1996, pp. 1701-1703.
- [18] Y. Chen, Z. Lin Wang, J. Song Yin, D.J. Johnson, and R.H. Prince, "Well-aligned graphitic nanofibers synthesized by plasma-assisted chemical vapor deposition," *Chemical Physics Letters*, vol. 272, Jun. 1997, pp. 178-182.
- [19] K. Hata, D.N. Futaba, K. Mizuno, T. Namai, M. Yumura, and S. Iijima, "Water-Assisted Highly Efficient Synthesis of Impurity-Free Single-Walled Carbon Nanotubes," *Science*, vol. 306, Nov. 2004, pp. 1362-1364.
- [20] S. Helveg, C. Lopez-Cartes, J. Sehested, P.L. Hansen, B.S. Clausen, J.R. Rostrup-Nielsen, F. Abild-Pedersen, and J.K. Nørskov, "Atomic-scale imaging of carbon nanofibre growth," *Nature*, vol. 427, Jan. 2004, pp. 426-429.
- [21] P.B. Amama, C.L. Pint, L. McJilton, S.M. Kim, E.A. Stach, P.T. Murray, R.H. Hauge, and B. Maruyama, "Role of Water in Super Growth of Single-Walled Carbon

- Nanotube Carpets," *Nano Letters*, vol. 9, Jan. 2009, pp. 44-49.
- [22] L. Ci, S. Manikoth, X. Li, R. Vajtai, and P. Ajayan, "Ultrathick Freestanding Aligned Carbon Nanotube Films," *Advanced Materials*, vol. 19, 2007, pp. 3300-3303.
- [23] T.V. Sreekumar, T. Liu, S. Kumar, L.M. Ericson, R.H. Hauge, and R.E. Smalley, "Single-Wall Carbon Nanotube Films," *Chemistry of Materials*, vol. 15, Jan. 2003, pp. 175-178.
- [24] P.M. Ajayan, L.S. Schadler, C. Giannaris, and A. Rubio, "Single-Walled Carbon Nanotube-Polymer Composites: Strength and Weakness," *Advanced Materials*, vol. 12, 2000, pp. 750-753.
- [25] T. Kuzumaki, K. Miyazawa, H. Ichinose, and K. Ito, "Processing of carbon nanotube reinforced aluminum composite," *Journal of Materials Research*, vol. 13, 1998, pp. 2445-2449.
- [26] E. Flahaut, A. Peigney, C. Laurent, C. Marlière, F. Chastel, and A. Rousset, "Carbon nanotube-metal-oxide nanocomposites: microstructure, electrical conductivity and mechanical properties," *Acta Materialia*, vol. 48, Sep. 2000, pp. 3803-3812.
- [27] P.M. Ajayan, O. Stephan, C. Colliex, and D. Trauth, "Aligned Carbon Nanotube Arrays Formed by Cutting a Polymer Resin--Nanotube Composite," *Science*, vol. 265, Aug. 1994, pp. 1212-1214.
- [28] H.D. Wagner, O. Lourie, Y. Feldman, and R. Tenne, "Stress-induced fragmentation of multiwall carbon nanotubes in a polymer matrix," *Applied Physics Letters*, vol. 72, Jan. 1998, pp. 188-190.
- [29] Z. Jia, Z. Wang, C. Xu, J. Liang, B. Wei, D. Wu, and S. Zhu, "Study on poly(methyl methacrylate)/carbon nanotube composites," *Materials Science and Engineering A*, vol. 271, Nov. 1999, pp. 395-400.
- [30] R. George, K. Kashyap, R. Rahul, and S. Yamdagni, "Strengthening in carbon nanotube/aluminium (CNT/Al) composites," *Scripta Materialia*, vol. 53, Nov. 2005, pp. 1159-1163.
- [31] E.T. Thostenson and T. Chou, "Aligned multi-walled carbon nanotube-reinforced composites: processing and mechanical characterization," *Journal of*

- Physics D: Applied Physics*, vol. 35, 2002, pp. L77-L80.
- [32] L. Chen, X. Pang, and Z. Yu, "Study on polycarbonate/multi-walled carbon nanotubes composite produced by melt processing," *Materials Science and Engineering: A*, vol. 457, May. 2007, pp. 287-291.
- [33] X. Gong, J. Liu, S. Baskaran, R.D. Voise, and J.S. Young, "Surfactant-Assisted Processing of Carbon Nanotube/Polymer Composites," *Chemistry of Materials*, vol. 12, Apr. 2000, pp. 1049-1052.
- [34] N.R. Raravikar, L.S. Schadler, A. Vijayaraghavan, Y. Zhao, B. Wei, and P.M. Ajayan, "Synthesis and Characterization of Thickness-Aligned Carbon Nanotube-Polymer Composite Films," *Chemistry of Materials*, vol. 17, Mar. 2005, pp. 974-983.
- [35] A.H. Barber, S.R. Cohen, and H.D. Wagner, "Static and Dynamic Wetting Measurements of Single Carbon Nanotubes," *Physical Review Letters*, vol. 92, May. 2004, p. 186103.
- [36] S. Fan, M.G. Chapline, N.R. Franklin, T.W. Tombler, A.M. Cassell, and H. Dai, "Self-Oriented Regular Arrays of Carbon Nanotubes and Their Field Emission Properties," *Science*, vol. 283, Jan. 1999, pp. 512-514.
- [37] L. Ci, R. Vajtai, and P.M. Ajayan, "Vertically Aligned Large-Diameter Double-Walled Carbon Nanotube Arrays Having Ultralow Density," *The Journal of Physical Chemistry C*, vol. 111, Jul. 2007, pp. 9077-9080.
- [38] E.T. Thostenson, W.Z. Li, D.Z. Wang, Z.F. Ren, and T.W. Chou, "Carbon nanotube/carbon fiber hybrid multiscale composites," *Journal of Applied Physics*, vol. 91, 2002, p. 6034.
- [39] B.Q. Wei, R. Vajtai, Y. Jung, J. Ward, R. Zhang, G. Ramanath, and P.M. Ajayan, "Microfabrication technology: Organized assembly of carbon nanotubes," *Nature*, vol. 416, Apr. 2002, pp. 495-496.
- [40] R. Andrews, D. Jacques, A.M. Rao, F. Derbyshire, D. Qian, X. Fan, E.C. Dickey, and J. Chen, "Continuous production of aligned carbon nanotubes: a step closer to commercial realization," *Chemical Physics Letters*, vol. 303, Apr. 1999, pp. 467-474.
- [41] R. Kamalakaran, M. Terrones, T. Seeger, P. Kohler-Redlich, M. Rühle, Y.A. Kim, T.

- Hayashi, and M. Endo, "Synthesis of thick and crystalline nanotube arrays by spray pyrolysis," *Applied Physics Letters*, vol. 77, 2000, p. 3385.
- [42] M. Mayne, N. Grobert, M. Terrones, R. Kamalakaran, M. Rühle, H.W. Kroto, and D.R.M. Walton, "Pyrolytic production of aligned carbon nanotubes from homogeneously dispersed benzene-based aerosols," *Chemical Physics Letters*, vol. 338, Apr. 2001, pp. 101-107.
- [43] X. Li, X. Zhang, L. Ci, R. Shah, C. Wolfe, S. Kar, S. Talapatra, and P.M. Ajayan, "Air-assisted growth of ultra-long carbon nanotube bundles," *Nanotechnology*, vol. 19, 2008, p. 455609.
- [44] X. Li, "Tailoring Vertically Aligned Carbon Nanotube Growth and Fabrication of Carbon Nanotube Membrane Filters," Rensselaer Polytechnic Institute, 2007.
- [45] P.M. Ajayan and J.M. Tour, "Materials Science: Nanotube composites," *Nature*, vol. 447, Jun. 2007, pp. 1066-1068.
- [46] L. Ci, J. Suhr, V. Pushparaj, X. Zhang, and P.M. Ajayan, "Continuous Carbon Nanotube Reinforced Composites," *Nano Letters*, vol. 8, 2008, pp. 2762-2766.
- [47] "Polydimethylsiloxane - Wikipedia, the free encyclopedia," Mar. 25, 2010. [Online]. Available: <http://www.en.wikipedia.org/wiki/Polydimethylsiloxane>. [Accessed: Mar. 25, 2010].
- [48] J.C. McDonald and G.M. Whitesides, "Poly(dimethylsiloxane) as a Material for Fabricating Microfluidic Devices," *Accounts of Chemical Research*, vol. 35, Jul. 2002, pp. 491-499.
- [49] S.R. Quake and A. Scherer, "From Micro- to Nanofabrication with Soft Materials," *Science*, vol. 290, Nov. 2000, pp. 1536-1540.
- [50] A. Galano, "Carbon Nanotubes as Free-Radical Scavengers," *The Journal of Physical Chemistry C*, vol. 112, Jun. 2008, pp. 8922-8927.